

## Accepted Manuscript

Structural conformations and density functional study on the intramolecular charge transfer based on vibrational spectra of 2,4-dihydroxy-*N'*-(4-methoxybenzylidene)benzohydrazide

D.M. Suresh, D. Sajan, Yun-Peng Diao, Ivan Němec, I. Hubert Joe, V. Bena Jothy

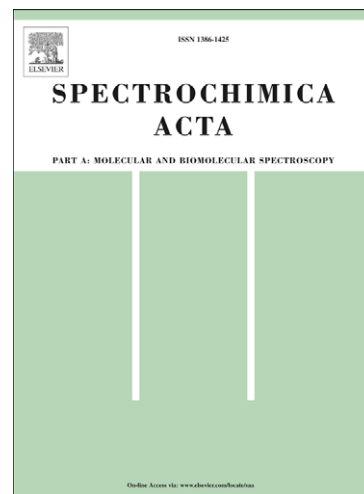
PII: S1386-1425(13)00105-4  
DOI: <http://dx.doi.org/10.1016/j.saa.2013.01.067>  
Reference: SAA 10217

To appear in: *Spectrochimica Acta Part A: Molecular and Biomolecular Spectroscopy*

Received Date: 5 October 2012  
Revised Date: 2 January 2013  
Accepted Date: 18 January 2013

Please cite this article as: D.M. Suresh, D. Sajan, Y-P. Diao, I. Němec, I. Hubert Joe, V. Bena Jothy, Structural conformations and density functional study on the intramolecular charge transfer based on vibrational spectra of 2,4-dihydroxy-*N'*-(4-methoxybenzylidene)benzohydrazide, *Spectrochimica Acta Part A: Molecular and Biomolecular Spectroscopy* (2013), doi: <http://dx.doi.org/10.1016/j.saa.2013.01.067>

This is a PDF file of an unedited manuscript that has been accepted for publication. As a service to our customers we are providing this early version of the manuscript. The manuscript will undergo copyediting, typesetting, and review of the resulting proof before it is published in its final form. Please note that during the production process errors may be discovered which could affect the content, and all legal disclaimers that apply to the journal pertain.



**Structural conformations and density functional study on the intramolecular charge transfer based on vibrational spectra of 2,4-dihydroxy-*N'*-(4-methoxybenzylidene)benzohydrazide**

**D.M .Suresh<sup>a,f</sup>, D. Sajan<sup>b,e\*</sup>, Yun-Peng Diao<sup>c#</sup>, Ivan Němec<sup>d</sup>, I. Hubert Joe<sup>e</sup>  
and V. Bena Jothy<sup>f,‡</sup>**

<sup>a</sup>*Government Arts College, Stone Hill House, Udthagamandalam, The Nilgiris - 643 002, Tamilnadu, India\*

<sup>b</sup>*Department of Physics, Bishop Moore College, Mavelikara, Alappuzha-690 110, Kerala, India.*

<sup>c</sup>*School of Pharmacy, Dalian Medical University, Dalian 116044, People's Republic of China*

<sup>d</sup>*Department of Inorganic Chemistry, Faculty of Science, Charles University in Prague, Albertov 2030, 128 40, Prague 2, Czech Republic*

<sup>e</sup>*Centre for Molecular and Biophysics Research, Department of Physics, Mar Ivanios College, Thiruvananthapuram-695 015, Kerala, India*

<sup>f</sup>*Department of Physics, Women's Christian College, Nagercoil, Tamil Nadu - 629001*

\*Corresponding author: Tel.:+91-9447000266; Fax: +91-479-2303230

E-mail address: \*[dsajand@gmail.com](mailto:dsajand@gmail.com), #[diaoyiwen@126.com](mailto:diaoyiwen@126.com),  
<sup>‡</sup>[benaezhil@yahoo.com](mailto:benaezhil@yahoo.com)

**ABSTRACT**

The NIR-FT Raman and FT-IR spectra of 2,4-dihydroxy-*N'*-(methoxybenzylidene) benzohydrazide (DMBBH) molecule have been recorded and analysed. Density functional theory (DFT) calculations at the B3LYP/6-31G(d) level has been used to compute energies of different conformers of DMBBH to find out their stability, the optimized geometry of the most stable conformer and its vibrational spectrum. Information about the size, shape, charge density distribution and site of chemical reactivity of the molecules has been obtained by mapping electron density isosurface with electrostatic potential

surfaces (ESP). A complete vibrational analysis has been attempted on the basis of experimental infrared and Raman spectra and calculated vibrational modes and potential energy distribution over the internal coordinates. The vibrational analysis confirm the charge transfer interaction between the phenyl rings through  $\text{>C=N-N<}$  skeleton. The broadening of the band at  $1631\text{cm}^{-1}$  and the appearance of the band at  $1556\text{cm}^{-1}$  strongly suggests the existence of proton equilibrium.

**Keywords:**, FT-IR ,FT-Raman spectra, DFT, NBO, Electrostatic potential

## 1. Introduction

Schiff base compounds, in addition to their role as versatile ligands in the field of coordination chemistry, can also act as important intermediates in many enzymatic reactions [1,2]. Due to the presence of an imine ( $-\text{N}=\text{CH}-$ ) group these compounds are susceptible to hydrolysis and transamination by nucleophiles [3]. The synthesis and physicochemical characterization of substituted aromatic Schiff base have received considerable attention since many of these compounds exhibit thermochromic and photochromic properties in the solid state by intramolecular proton transfer associated with a change in the  $\pi$ -electron configuration [4,5]. Some Schiff base metal complexes have been found to have pharmacological and antitumor properties [6,7], and can be used as model for biological systems [8]. The resistance reversal properties of some Schiff base compounds and metal complexes, their *in vitro* toxicity against cancer cells and

efficiency in slowing leukemia cell growth have also been reported in the literature [9]. Though the crystal structure of the title compound, 2,4-dihydroxy-*N'*-(4-methoxybenzylidene) benzohydrazide (DMBBH) has been reported [10], the vibrational spectral features of DMBBH crystal have not been subject of detailed analysis so far. NIR-FT Raman spectra combined with quantum chemical computations have recently been effectively applied in the vibrational analysis of drug molecules [11,12], biological compounds [13], natural products [14] and NLO active compounds [15-17], since fluorescence free Raman spectra and computed results help with unambiguous identification of vibrational modes and provide deeper insight into the bonding and structural features of complex organic molecular systems. The present work reports the detailed vibrational spectral analysis of 2,4-dihydroxy-*N'*-(4-methoxybenzylidene) benzohydrazide molecule (Figure 1) to elucidate the correlation between the molecular structure and prediction of normal modes, to understand the structural and bonding features, photon transfer equilibrium, the intramolecular interactions and factors influencing the vibrational spectrum of the molecule supported using the scaled quantum mechanical (SQM) force field technique based on density functional theory.

## **2. Experimental**

### **2.1 Synthesis of the compound**

4-Methoxybenzaldehyde and 2,4-dihydroxybenzoic acid hydrazide were dissolved in ethanol and the mixture was stirred at room temperature to give a clear colourless solution. Crystals of 2,4-dihydroxy-*N'*-(4-methoxybenzylidene) benzohydrazide were formed by slow evaporation of the solvent over a period of three days at room temperature.

## 2.2. IR and Raman measurements

FT-IR spectra of the title compound were recorded on Thermo Nicolet Magna 760 FTIR spectrometer by DRIFTS (Diffuse Reflectance Infrared Fourier Transform Spectroscopy) technique. The samples were mixed with KBr and scanned in 400-4000  $\text{cm}^{-1}$  wavenumber range (Happ-Genzel apodization, 2  $\text{cm}^{-1}$  resolution) using Pike Technology EasiDiff accessory. The Raman spectra of polycrystalline samples and ethanol solution were collected on the same spectrometer equipped with Thermo Nicolet Nexus FT-Raman module. The measurements were carried out in the range of 100-3700  $\text{cm}^{-1}$  (Happ-Genzel apodization, 2  $\text{cm}^{-1}$  resolution, 1064 nm Nd:YVO<sub>4</sub> laser excitation, 450 mW power at the sample). Both IR and Raman spectra were processed using the OMNIC software [18].

## 3. Computational details

All *ab initio* molecular orbital calculations were carried out using the Gaussian'03 program package [19]. Initially, the structure of DMBBH molecule

were optimized, and then the vibrational wavenumbers were calculated with the B3LYP method using the 6-31G(d) basis set. At the optimized structure of the DMBBH, no imaginary frequency modes were obtained, proving that a true minimum on the potential energy surface was found. The optimum geometry was determined by minimizing the energy with respect to all geometrical parameters without imposing molecular symmetry constraints. The inclusion of 'd' polarization and double-zeta function in the split valence basis set is expected to produce a marked improvement in the calculated geometry [20]. The DFT hybrid B3LYP functional tends to overestimate the fundamental modes in comparison to the other DFT method, therefore scaling factors have to be used for obtaining a considerably better agreement with experimental data. Isoelectronic molecular electrostatic potential surfaces (MEPSs) and electron density surfaces were calculated using 6-311G(d,p) basis set with (83,83,52) grid points with an average resolution of 0.333 Bohr. Structures resulting from the plot of electron density surface mapped with electrostatic potential surface depict the shape, size, charge density and the site of chemical reactivity of a molecule. These surfaces were plotted by the computer software Gauss View 5.0. The vibrational modes were assigned on the basis of PED analysis using VEDA 4 program [21] and its visualization interface. Normal coordinate analysis of the title molecule has been carried out to obtain a more complete description of the molecular motions involved in the fundamentals. The calculated vibrational wavenumbers were

scaled [22] with the scale factors, which accounts for systematic errors caused by the basis set incompleteness, neglect of electron correlation and vibrational anharmonicity. The Raman activities ( $S_i$ ) calculated by the Gaussian-03 program have been converted to relative Raman intensities ( $I_i$ ) using the following relationship derived from the basic theory of Raman scattering [23].

$$I_i = \frac{f(\nu_o - \nu_i)^4 S_i}{\nu_i \left[ 1 - \exp\left(\frac{-hc\nu_i}{kT}\right) \right]} \quad (1)$$

where  $\nu_o$  is the exciting frequency (in  $\text{cm}^{-1}$  units),  $\nu_i$  is the vibrational wavenumber of the  $i^{\text{th}}$  normal mode,  $h$ ,  $c$  and  $k$  are universal constants, and  $f$  is the suitably chosen common scaling factor for all the peak intensities.

## 4. Results and discussion

### 4.1 Crystal structure

As it was previously reported [10], DMBBH crystallizes in orthorhombic space group,  $Pna2_1$ . The cell dimensions are  $a=12.494(3)$  Å,  $b=5.196(1)$  Å,  $c=20.825(4)$  Å and  $V=1351.9(5)$  Å<sup>3</sup>. The title molecule displays a *trans* configuration with respect to the C=N bond. The dihedral angle between the two benzene rings is  $15.0(2)^\circ$ . The molecular conformation is stabilized by the intramolecular N-H...O interaction. In the crystal, molecules are linked through

intermolecular O-H...N and O-H...O hydrogen bonds, forming layers parallel to the *ab* plane.

#### 4.2. Conformational analysis

With B3LYP/6-31G(d) level the conformational analysis was done by changing the torsional angle  $\theta$  by  $10^\circ$  steps between  $\theta = 0^\circ$  (syn form) and  $\theta = 180^\circ$  (anti form) to analyze the stability of the molecule. For each conformer, the dihedral angle was held fixed while the remainder of the molecule was optimized (the rigid rotor approximation was not applied). The two conformers of DMBBH molecule, which have been optimized at B3LYP/6-31G(d) level, are shown in Fig.1(a) & (b). The optimized energy of conformers are predicted at  $-2.60025 \times 10^6$  KJ/mol (conformer 1) and  $-2.60024 \times 10^6$  KJ/mol (conformer 2). The relative energy is determined at 0.00001 KJ/mol for conformer 2 (Fig.1a & 1b). The results show that conformer 2 is more stable than the conformer 1.

Figure-1

Potential energy surface scan studies have been carried out in order to ascertain its *trans* (Fig.1b) form due to paucity in reliable experimental structural data and for the popular notion that the *trans* form is more stable [10]. The results obtained in PES scan studies by varying the torsional perturbation of  $\tau$  C<sub>1</sub>-C<sub>14</sub>-N<sub>16</sub>-N<sub>18</sub> with step angle of  $10^\circ$  are plotted in figure -2. The calculated molecular energy at  $180.0^\circ$  torsion angle, ( $\tau$ C<sub>1</sub>-C<sub>14</sub>-N<sub>16</sub>-N<sub>18</sub>) is about  $-2.60024 \times 10^6$  KJ/mol which is larger than that of the *cis* conformation.

- Figure-2

The energy barrier of rotation around the O<sub>31</sub>-C<sub>24</sub> bond was calculated for the B3LYP with 6-31G(d) basis sets. The dihedral angles of C<sub>25</sub>-C<sub>24</sub>-O<sub>31</sub>-C<sub>32</sub> (around O<sub>31</sub>-C<sub>24</sub> bond) were varied from 0° to 180° by steps of 10°. The energy profile obtained from DFT method (Fig-3) as a function of  $\varphi$  has shown the minimum at 0° and the maximum at 180°. The minimum positions were corresponding to the *trans* conformer and the maximum positions were corresponding to the *cis* conformer.

- Figure-3

The O<sub>7</sub>-H<sub>13</sub> group favour planar conformation (figure -4a) due to the energy minimum at 0/360° predicted by energy profile. This is because of the Van der Waals' repulsion between H<sub>17</sub> and H<sub>13</sub>. The PES scan results reveal that the molecule exists in *trans*-configuration, which is important for its bioactivity. From the graph (figure-4b) the energy minimum for O<sub>9</sub>-H<sub>10</sub> P<sub>z</sub> -orbital oxygen lone pair conjugation of O<sub>9</sub> and  $\pi$ -system of resorcinol group is maximum leading to the conclusion that possibility of perpendicular conformation of O<sub>9</sub>-H<sub>10</sub> with respect to the resorcinol group is rejected. The local minimum at 180° is less favored compared to planar conformation which is due to the possible steric effect arising from the Van der Waals' repulsion between H<sub>8</sub> and H<sub>10</sub> (H<sub>8</sub>····H<sub>10</sub>=2.28 Å) and H<sub>11</sub> and H<sub>10</sub> (H<sub>10</sub>····H<sub>11</sub>=2.29Å).

#### 4.3 Natural bond orbital (NBO) analysis

The NBO analysis was performed with the NBO 5.0 program [24]. A short outline of the NBO segments used and their structural meaning is presented below. NBO theory allows the assignment of the hybridization of atomic lone pairs and of the atoms involved in bond orbitals. These are the important data in spectral interpretation since the frequency ordering is related to the bond hybrid composition. The NBO analysis allows us to estimate the energy of the molecule with the same geometry but in the absence of electronic delocalization. Moreover, only the steric and electrostatic interactions through the  $E_{\text{Lewis}}$  are taken into account. The most important interactions between ‘filled’ (donor) Lewis-type NBOs and ‘empty’ (acceptor) non-Lewis NBOs are reported in Table 1. The stabilization energy  $\Delta E_{ij}$  associated with delocalization is estimated using the second-order perturbation theory as:

$$E(2) = -n_{\sigma} \frac{\langle \sigma | F | \sigma \rangle^2}{\epsilon_{\sigma^*} - \epsilon_{\sigma}} = -n_{\sigma} \frac{F_{ij}^2}{\Delta E} \quad (2)$$

where  $\langle \sigma | F | \sigma \rangle^2$  or  $F_{ij}^2$  is the Fock matrix (Kohn–Sham matrix) element between the  $i$  and  $j$  NBO orbitals,  $\epsilon_{\sigma}$  and  $\epsilon_{\sigma^*}$  are the energies of  $\sigma$  and  $\sigma^*$  NBO's, and  $n_{\sigma}$  is the population of the donor  $\sigma$  orbital.

The second-order perturbation theory analysis of Fock matrix in NBO shows strong intramolecular hyperconjugative interactions, which are presented in Table 1. The intramolecular hyperconjugative interactions are formed by the

orbital overlap between  $\pi$  (C–C) and  $\pi^*$ (C–C) bond orbitals which results intramolecular charge transfer (ICT) causing stabilization of the system [25,26]. The hyperconjugative interaction between  $LP_1 N_{16} \rightarrow \pi^* (C_{14}-O_{15})$  [ 243.1  $KJmol^{-1}$  ],  $LP_1 N_{16} \rightarrow \pi^* (N_{18}-C_{19})$  [ 121.1  $KJmol^{-1}$  ],  $LP_2 O_9 \rightarrow \pi^* (C_4-C_5)$  [ 132.6  $KJmol^{-1}$  ],  $LP_2 O_{31} \rightarrow \pi^* (C_{23}-C_{25})$  [ 129.3  $KJmol^{-1}$  ] and  $LP_2 O_{15} \rightarrow \sigma^* (C_{14}-N_{16})$  [ 116.6  $KJmol^{-1}$  ] have higher values than the other delocalizations.

- Table-1

#### 4.4 Geometry and Electronic Structure

The optimized structural parameters of DMBBH are listed in Table 2. The corresponding values obtained from X-ray diffraction pattern are also given in the table for comparison. From the Table 2 it can be seen that there are small deviations in the computed geometric parameters from those obtained from the XRD data [10]. These deviations can be attributed to the fact that the theoretical calculations have been carried out with isolated molecules in the gaseous phase and the experimental values correspond to molecules in the crystalline state. As evident from the observed  $N_{18}-C_{19}$  bond distance of 1.270 Å, this is consistent with an N=C double bond. The  $C_{21}-C_{19}-N_{18}-N_{16}$  torsion angle [178.5°] shows a *trans* configuration about the  $C_{19}-N_{18}$  bond. The  $C_4-O_9$  and  $C_6-O_7$  bond lengths of 1.366 Å are consistent with the C-O single bond distances reported in analogous structures [7,27]. The molecular conformation is stabilized by an intramolecular

N-H...O hydrogen bond interaction [2.7191 Å]. A short intramolecular hydrogen bond associated with the charge flow through the system of conjugated double bond is denoted as resonance-assisted hydrogen bonding [28] and a delocalization parameter,  $Q$ , defined as  $Q = (d_1 - d_4) + (d_3 - d_2)$ , where  $d_1, d_2, d_3$  and  $d_4$  are C<sub>6</sub>-O<sub>7</sub>[1.366 Å], C<sub>6</sub>-C<sub>1</sub>[1.405 Å], C<sub>1</sub>-C<sub>14</sub>[1.483 Å] and C<sub>14</sub>-N<sub>16</sub>[1.340 Å] bond lengths respectively. The positive sign of  $Q$  value [0.104 Å] in the title compound is a consequence of the electron withdrawing of resorcinol substituent group and is in agreement with other crystallographic structures [29]. In the crystal, molecules are linked through intermolecular O-H...N and O-H...O hydrogen bonds, forming layers parallel to the *ab* plane.

- Table-2

The net charges of the atoms in the title compound calculated at the B3LYP/6-31G (d) level are shown in the figure-5. The oxygen and nitrogen atoms in the molecule bear negative charges; the phenyl ring carbon atoms with substituent (i.e. C<sub>4</sub>, C<sub>6</sub>, C<sub>1</sub>, C<sub>21</sub> and C<sub>24</sub>), the carbonyl carbon C<sub>14</sub> and bridging C<sub>19</sub> atom bear positively charges while the remaining carbon atoms of the phenyl rings bear negative charges. The large electron density at the phenolic O atoms (O<sub>7</sub> and O<sub>9</sub>) suggests possible protonation at O<sub>7</sub> and O<sub>9</sub>. Due to this charge distribution, the dipole of the molecule becomes 5.663 Debye.

- Figure-5

The orbital energy level analysis for DMBBH at the B3LYP/6-31G(d) level shows  $E_{\text{HOMO}}$  (highest occupied molecular orbital) and  $E_{\text{LUMO}}$  (lowest unoccupied molecular orbital) values of -0.31156 eV and -0.20753 eV, respectively. The magnitude of the HOMO-LUMO energy separation could indicate the reactivity pattern of the molecule. The charge densities for the HOMO and LUMO are shown in Figure-6. For the HOMO and LUMO in DMBBH there is very little charge density on the hydrogen atoms. The HOMO is located on the  $C_{21}-C_{22}$ ,  $C_{21}-C_{26}$ ,  $C_{24}-C_{25}$  and  $C_{24}-C_{23}$  bonds of the phenyl ring (*p*-methoxybenzylidene) as well as on the oxygen atoms of hydroxyl ( $O_6$  and  $O_9$ ), carbonyl oxygen ( $O_{15}$ ), methoxy group ( $O_{31}$ ) and the nitrogen ( $N_{16}$  and  $N_{18}$ ) atoms, with only minor population on the other phenyl ring (resorcinol). The LUMO in DMBBH, however, populates on the carbon atoms ( $C_{22}$ ,  $C_{24}$  and  $C_{26}$ ) of the phenyl ring (*p*-methoxybenzylidene),  $C_2$ ,  $C_4$ ,  $C_5$  and  $C_6$  atoms of the phenyl ring (resorcinol), carbonyl group ( $C_{14}=O_{15}$ ), methoxy group ( $O_{31}$ ) and the nitrogen ( $N_{18}$ ) atoms, but with only minor population on the oxygen atoms of hydroxyl ( $O_6$  and  $O_9$ ). The population of LUMO on the bonding between  $C_{22}-C_{23}$ ,  $C_{19}-C_{21}$ ,  $C_1-C_{14}$  and  $C_4-C_3$  forms antibonding orbitals. Minor population is located on the oxygen atoms on the methoxy groups. The difference between the orbital energies corresponding to HOMO-1 (-0.34296 eV) and HOMO-2 (-0.35718 eV) is much higher than 0.05 eV indicating that the HOMO-1 and HOMO-2 are

nondegenerate in DMBBH. Similar conclusion can be drawn from the LUMO+1 and LUMO+2 orbital energy calculations.

- Figure-6

According to molecular orbital energy, HOMO and LUMO are the two important factors influencing the bioactivity. The interaction between the title compound and the receptor can be dominated by  $\pi$ - $\pi$  or hydrophobic interaction among these frontier molecular orbitals. The negative charges mainly located on O<sub>7</sub>, O<sub>9</sub>, O<sub>15</sub>, N<sub>16</sub>, N<sub>18</sub> and O<sub>31</sub> are likely to interact with positive part of the receptor. On the contrary, the most positively charged part will interact quite easily with negatively charged part of the receptor. These interactions can play crucial role in bioactivity.

#### 4.5 Molecular electrostatic potential

The ESP,  $V(\mathbf{r})$ , at a point  $\mathbf{r}$  due to a molecular system with nuclear charges  $\{Z_A\}$  located at  $\{R_A\}$  and electron density  $\rho(r)$  is given by

$$V(r) = \sum_{A=1}^N \frac{Z_A}{|r - R_A|} - \int \frac{\rho(r') d^3 r'}{|r - r'|} \quad (3)$$

The graphical representation of the molecular electrostatic potential surface (MEP or ESP), as described by Kollman and Singh[30] is a series of values representing the evaluation of the interaction energy between a positively charged (proton) probe and points on a solvent accessible surface as defined by

Connolly[31]. As implemented within the Gauss View ver.4.1 program, areas of high electron density, representing a strong attraction between the proton and the points on the molecular surface, have the brightest red color and areas of lowest electron density; have deep blue to indigo color, indicating the regions of maximum repulsion.

Molecular electrostatic potential (ESP) at a point in the space around a molecule gives an indication of the net electrostatic effect produced at that point by the total charge distribution (electron + nuclei) of the molecule and correlates with dipole moments, electro negativity, partial charges and chemical reactivity of the molecules. It provides a visual method to understand the relative polarity of the molecule. An electron density isosurface mapped with electrostatic potential surface depicts the size, shape, charge density and site of chemical reactivity of the molecules. The different values of the electrostatic potential at the surface are represented by different colours; red represents regions of most negative electrostatic potential, blue represents regions of most positive electrostatic potential and green represents regions of zero potential. The potential increases in the order red < orange < yellow < green < blue. Projections of these surfaces along the molecular plane are given in Figure- 7. This figure provides a visual representation of the chemically active sites and comparative reactivity of atoms.

- Figure-7

It may be seen that, in both the molecules, a region of zero potential envelopes the  $\pi$ -system of the benzene rings, leaving a more electrophilic region in the plane of the hydrogen atoms. The shape of the electrostatic potential surfaces at sites close to the polar carbonyl group in the molecule and the hydrazide group is influenced by the stereo structure and the charge density distribution. These sites show regions of most negative electrostatic potential and high activity of the carbonyl and hydrazide group. In contrast, regions close to the other two polar atoms – oxygen of the phenyl ring and oxygen of the methoxy group – show regions of mildly negative and zero potential, respectively.

Another quantity of utility in the analysis of intrinsic reactivity is the local ionization potential (IP),  $I(r)$ . This is defined as the sum over orbital electron densities,  $\rho_i(r)$  times the absolute orbital energies,  $|\epsilon_i|$  and divided by the total electron density  $\rho(r)$ ,

$$I(r) = \frac{\sum_i^{\text{occupied molecular orbitals}} \rho_i(r) |\epsilon_i|}{\rho(r)}$$

The local IP is intended to reflect the relative ease of electron removal at any location around a molecule [32-34]. Thus, as we use it here, it is a measure of the susceptibility of a molecular region to electrophilic attack (reactivity). The surface mapped values of the IP, as derived from Gauss View ver.4.1 program are shown in Fig.7. The graphical convention used (Fig.7,) indicates a range of

relative values, with red representing regions of highest likelihood of electrophilic attack, and blue, at the other extreme, areas of lowest likelihood (most nucleophilic regions).

#### 4.6 Vibrational spectral analysis

The vibrational analysis of DMBBH is performed on the basis of the characteristic vibrations of resorcinol, hydrazide and methoxybenzilidine groups. Theoretical calculations were performed using density functional theory with B3LYP/6-31G(d) basis set. The computed vibrational wavenumbers and the atomic displacements corresponding to different normal modes are used for identifying the vibrational modes unambiguously. The detailed vibrational assignments of fundamental modes along with the calculated infrared and Raman intensities and normal modes description (characterized by PED) are reported in Table 3. For visual comparison, the observed and simulated FT-IR and FT-Raman spectra are presented in figures-8 & 9. The calculated spectra are found to be close to the experimental values with reasonable accuracy. H-atoms involved in intermolecular H-bonds shows deviation in the simulated spectra, which is attributed to the fact that the theoretical spectrum was obtained in gas phase without considering the inter-molecular H-bonding effects. Vibrational spectral analysis of the phenyl rings are different as expected due to their substitution and they are comprehensively studied according to Wilson's numbering convention [35].

- Table-3
- Figure-8&9

#### 4.6.1 Resorcinol group vibrations

The major vibrational modes of resorcinol are derived from phenyl ring and hydroxyl groups. The hydroxyl stretching and bending bands can be identified by their broadness and strength of the band which is dependent on the extent of hydrogen bonding. Vibrational absorption spectra provide information about the local properties of hydrogen-bonded groups. The line shapes of the high-wavenumber O–H stretching mode involved in the hydrogen bonds are often very complex and highly congested, reflecting the complicated underlying microscopic interactions, and consequently, the dynamics and line broadening mechanisms of hydrogen bonds. Formation of a hydrogen bond  $X-H\cdots Y$  between a hydrogen donor  $X$  and hydrogen acceptor  $Y$  leads to pronounced changes in the high-wavenumber X-H stretching modes [36-38]. The non-hydrogen bonded or free hydroxyl group absorbs strongly in the  $3700-3600\text{ cm}^{-1}$  region while the existence of intermolecular hydrogen bond can lower the O-H stretching wavenumber in the  $3550-3200\text{ cm}^{-1}$  region with the increase in IR intensity and broadness. In IR spectrum the hydroxyl stretching bands splits into two bands at  $3200\text{ cm}^{-1}$  and  $3250\text{ cm}^{-1}$  corresponding to  $O_7-H_{13}$  and  $O_9-H_{10}$  stretching vibrations. The DFT computations give the wavenumber of these bands at  $3581\text{ cm}^{-1}$  (100 %) and  $3587\text{ cm}^{-1}$  (100 %) for  $O_7-H_{13}$  and  $O_9-H_{10}$  stretching

vibrations. The appearance of the red shift of the  $O_9-H_{10}$  and  $O_7-H_{13}$  stretching wavenumber is clearly due to the formation of a intermolecular and  $H_{17}\dots O_7-H_{13}$  intramolecular hydrogen bond respectively. Interaction of lone pairs of oxygen (electron donor) with the O-H antibonding  $\sigma^*$  orbital leads to an increase of electron populations in this orbital, followed by a weakening of the O-H bond which results in the lowering of O-H stretching wavenumber. The computed results suggest the possibility of intra molecular effects. The H-O---H distances being:  $H_{13}\dots H_{17}=2.785 \text{ \AA}$ . The intramolecular interactions are obviously weaker and the above interactions throw off the expected values of band positions, computed using DFT. The above mentioned interactions are expected to weaken the bonds, thereby reducing  $O_7-H_{13}$  stretching force constant which is manifested as the lowering of the experimental stretching wavenumber from the computed values. Also the observed  $O_9-H_{10}$  and  $O_7-H_{13}$  stretching wavenumbers are lowered from the computed wavenumbers due to the intermolecular O-H---O hydrogen bond interaction, justified by XRD data. The in plane bending O-H deformation vibration usually appears as a strong band in the region  $1440-1260 \text{ cm}^{-1}$  in the IR spectrum, which gets shifted to higher wavenumbers due to the presence of hydrogen bonding. The O-H in-plane bending vibration is observed at  $1463 \text{ cm}^{-1}$  as medium IR band together with  $CH_3$  bending modes. The O-H in plane bending mode appears in our calculations at  $1473 \text{ cm}^{-1}$  with a composition of 60 %  $\delta HOC$  and  $\delta CH_3_{asy}$  (22 %). The O-H out of plane bending vibration

gives rise to a broad band in the region  $800\text{-}600\text{ cm}^{-1}$ . The weak band at  $790\text{ cm}^{-1}$  in the infrared spectrum is attributed to the O-H out of plane bending mode. The band correlated with O-H torsional mode was identified at  $463\text{ cm}^{-1}$  in infrared spectra.

In resorcinol group, the phenyl ring is asymmetrically tri substituted. The C-H stretching wavenumber of tri substituted benzene is expected in the region  $3000\text{ - }3100\text{ cm}^{-1}$  [36-38]. These are  $3091$ ,  $3078$  and  $3008\text{ cm}^{-1}$  vibration, in which only the C-H bonds of the  $\text{Ph}_2$  ring participate. The selection rule allows all the three bands 2, 20a and 20b modes of C-H stretching [35]. But 2 and 20b is absent or mixed with very broad band of hydroxyl stretch in that region which cannot be distinctly observed. The ring mode 20a can be observed in IR at  $3074\text{ cm}^{-1}$  and in Raman at  $3076\text{ cm}^{-1}$ .

For asymmetrically tri substituted benzene and its derivatives, the modes 1, 8a, 8b, 19a, 19b and 14, are allowed for tangential C-C stretch [35]. The mode 8b appears in calculation at  $1609\text{ cm}^{-1}$  with a composition of 51% 8b. The experimental value of this wavenumber is  $1609\text{ cm}^{-1}$  in Raman spectra, which indicates an excellent agreement with the calculations. The 8a modes appear at lower wavenumber of  $1582\text{ cm}^{-1}$  with a composition of 50% 8b. The ring mode 8a can be observed as very strong bands at  $1576\text{ cm}^{-1}$  (IR) and  $1574\text{ cm}^{-1}$  (Raman and solution Raman). The 19b mode is found having considerable contribution to this mode, appearing at  $1500\text{ cm}^{-1}$ , which is mixed with 11%  $\nu_{\text{CC}}$  and 33 %  $\delta_{\text{CCH}}$ ,

and cannot be distinctly observed experimentally. The 19a mode is attributed to  $1433\text{ cm}^{-1}$ , with significant contribution of 41%  $\nu_{\text{CC}}$ . The mode 19a is found as medium bands at  $1424\text{ cm}^{-1}$  in IR, Raman and solution Raman spectrum. Mode 14 was assigned to the wavenumber of  $1307\text{ cm}^{-1}$ , since it has a composition of 57%  $\nu_{\text{CC}}$  and 26%  $\delta_{\text{HOC}}$ . The weak band observed at  $1335\text{ cm}^{-1}$  (IR) corresponds to the 14 mode.

The normal vibrations 3, 15 and 18b are classified as C-H in-plane bending vibrations [35]. The strong bands observed at  $1258\text{ cm}^{-1}$  (IR),  $1257\text{ cm}^{-1}$  (solution Raman) and  $1259\text{ cm}^{-1}$  (Raman) are assigned to mode 3. The medium IR band appearing at  $1193\text{ cm}^{-1}$  is attributed to vibrational mode 15. The mode 18b is coupled with the CCC bending mode and is found active in the Raman spectrum at  $1073\text{ cm}^{-1}$  as a medium band and in the IR spectrum at  $1074\text{ cm}^{-1}$ . The normal modes 10a, 10b and 11 which allow C-H out-of-plane bending vibrations, are expected in the region  $960\text{-}780\text{ cm}^{-1}$  [37-39]. The mode 10a is observed in the IR at  $950\text{ cm}^{-1}$  and the calculated wavenumber is  $958\text{ cm}^{-1}$  (32% PED). The weak bands observed in the IR at  $807\text{ cm}^{-1}$  and in the Raman spectrum at  $808\text{ cm}^{-1}$  are assigned to 10b mode. The radial skeletal (1, 6a and 6b) and the out-of-plane skeletal (4, 16a and 16b) vibrations are listed in Table 3.

#### 4.6.2 Hydrazide group vibrations

The vibrational analysis of hydrazide is performed based on the characteristic vibrations of amide group, C-N and N-N groups. The secondary

amides exhibit bands due to the N-H stretching and deformation vibrations. The positions of the NH stretching and deformation bands are dependent on the strength of hydrogen bond formed. The free NH stretching modes of secondary amides are generally observed in the region 3550-3250  $\text{cm}^{-1}$  for the N-H stretching mode and a weak band at 3100-3070  $\text{cm}^{-1}$  for the overtone of the N-H bending [36-40]. The N-H stretching modes are observed as a medium broad band in the IR spectrum at 3160  $\text{cm}^{-1}$ . The DFT computations give the wavenumber of this band at 3352  $\text{cm}^{-1}$  (100% N-H) for the N-H stretch. The red-shifting of the N-H stretching wavenumbers are due to the formation of inter- and intramolecular N-H...O hydrogen bonds. The calculated geometry  $\text{H}_{17}\dots\text{O}_7$  (1.922 Å),  $\text{N}_{11}\dots\text{O}_{19}$  (2.719 Å) and  $\text{N}_{16}\text{-H}_{17}\dots\text{O}_7$  (132.82°) supports the intramolecular N-H...O hydrogen bonding. From Table 1 it is evident that the ED in  $\text{N}_{16}\text{-H}_{17}$  antibonding  $\sigma^*$  orbital was significantly increased (0.8750 e) by the strong hydrogen bond between N-H group ( $\text{N}_{16}\text{-H}_{17}$ ) and lone pair of  $\text{O}_7$  in the molecule providing unambiguous evidence about the weakening of the bond, its elongation (116.1 pm) and concomitant red shift of the N-H stretching wavenumber. The stabilization energy  $E^{(2)}$  associated with hyperconjugative interaction  $\text{LP}(\text{O}_7) \rightarrow \sigma^*(\text{N}_{16}\text{-H}_{17})$  is obtained as (37.45 kJ/mol). It is noteworthy that the N-H bond order correlates with the calculated N...O distance, by increasing the hydrogen bond strength, reducing the N...O distance, the N-H bond order decreases.

The N-H in- plane deformation vibrations normally appear in the region 1650-1550  $\text{cm}^{-1}$  [36-39]. The weak band at 1536  $\text{cm}^{-1}$  in IR spectra corresponds to the N-H in-plane deformation mode, which is coupled with the CCH bending, as revealed by PED calculations. The DFT computation gives the wavenumber at 1548  $\text{cm}^{-1}$  has 47 % N-H in-plane bending character because of its association with the 14 % CCH bending modes. The N-H out-of-plane bending mode can be observed as a weak band in IR and Raman at 572  $\text{cm}^{-1}$  and 571  $\text{cm}^{-1}$  respectively, whereas the computed value is 596  $\text{cm}^{-1}$  (325). The C-N stretching vibrations generally occur in the region 1170-1040  $\text{cm}^{-1}$ . The C-N stretching wavenumber was calculated to be 1024  $\text{cm}^{-1}$  (27 % PED) and the corresponding IR band is found at 1024  $\text{cm}^{-1}$ , which is coupled with N-N stretching mode (37 % PED).

Carbonyl vibrations are considered to give rise to characteristic bands in the vibrational spectrum and, for this reason, such bands have been subject of extensive studies [36-40]. The intensity of these bands can increase owing to the conjugation or formation of hydrogen bonds. The increase of conjugation, therefore, leads to an intensification of the Raman lines as well as increased infrared band intensities. Carbonyl stretching vibrations generally appear in the region 1750-1600  $\text{cm}^{-1}$ . The broad, intense IR band at 1631  $\text{cm}^{-1}$  corresponds to the C=O stretching vibration. The DFT computation gives the C=O stretching wavenumber of this mode as 1695  $\text{cm}^{-1}$  (63 % PED). The carbonyl stretching

mode is simultaneously influenced by the conjugation of C=O with amide nitrogen and mesomeric effect. When a nitrogen, oxygen or chlorine is attached to a carbonyl carbon, the nonbonding electrons on the attached atom N can rearrange and donate electrons to the carbonyl oxygen  $O=C-N \leftrightarrow O^-C=N^+$ . This weakens the C=O force constant depending on the electron donation tendency of N. In DMBBH it is a dominant effect, as the C=O stretching wavenumber is lower than that of ketones ( $1715\text{ cm}^{-1}$ ), even though the nitrogen is more electronegative than a carbon. This is justified by DFT calculation also. The unusual lowering of the carbonyl stretching wavenumber is also contributed by the electron releasing effect of the C=O bond in the acceptor subunit due to intramolecular charge transfer, as reported earlier [15-18] in addition to the intermolecular effect and  $\pi$ -conjugation. This mechanism plays an important role in the biological activity of DMBBH. The broadening of the band at about  $1631\text{ cm}^{-1}$  and the appearance of the band at  $1556\text{ cm}^{-1}$  strongly suggests the existence of proton equilibrium.

In phenyl hydrazones the possibility of obtaining a charge transfer interaction is related to the absence of even the slight amount of strain in the hydrazo group, which must be perfectly planar to allow conjugation of the group. The C=N stretching mode can be used as a good probe for evaluating the bonding configuration around the amino N atom and the electronic distribution of the aromatic amine compounds [40-41]. The C=N stretching appears in the region

1670-1630  $\text{cm}^{-1}$  [39]. The C=N stretching wavenumber is found to have considerable contribution to this mode and is appearing at 1624  $\text{cm}^{-1}$ , which is mixed with 32 %  $\nu_{\text{C18=N19}}$  and 40 %  $\nu_{\text{C-C}}$ . This cannot be distinctly resolved experimentally. The downshifting of C=N stretching wavenumber is due to the charge transfer interaction between the phenyl rings through  $\text{>C=N-N<}$  skeleton. The charge transfer interaction is related to the presence of at least one H atom bonded to the atoms of the phenylhydrazone skeleton ( $\text{>C=N-N<}$ ). The C=N stretching vibration is observed as a medium band at 1240  $\text{cm}^{-1}$  (Raman) and at 1241  $\text{cm}^{-1}$  (Solution Raman). According to PED calculations, vibrational mode C=N has only 20 % C=N stretching contribution and 16 % C-C stretching character.

#### 4.6.3 *p*-Methoxybenzylidene group vibrations

The methoxy group vibrations are observed as intense bands in both IR and Raman, but with large variation from the normal values of methyl groups. This must be due to the electronic effect caused by the presence of oxygen atoms, which causes a deviation from the expected values [38-39]. The vibrational modes of methoxy groups in DMBBH are known to be influenced by a variety of interesting interactions such as electronic effects and conjugation. For methoxy-substituted phenyl groups, the conjugation of the lone pair of oxygen with the  $p_z$  orbital of the aryl ring and the back donation are two competitive effects whose

relative weights determine the conformation dependent molecular properties [15-18]. The internal rotation of the  $\text{OCH}_3$  group can be described in terms of an angle  $\varphi$  between the plane of the ring and the plane containing  $\text{C}_{ar}$ , O and  $\text{C}_{me}$  atoms. Two effects influence the internal rotation about the  $\text{C}_{ar}$ -O axis are (i) the steric repulsion between the methyl hydrogen and the hydrogen at the adjacent position of the ring and (ii) the conjugation of the oxygen atom with ring. During the methoxy rotation, the conjugation of the oxygen lone pair with the aryl  $p_z$  orbital changes, reaching a maximum when the carbon atom of the methoxy group lies in the plane of the ring ( $\varphi = 0^\circ$ ). In DMBBH the methoxy carbon atom lies in the ring plane ( $\varphi = 0.001^\circ$ ), the induction effect is prominent. Induction produces stronger polarization of C-H bonds along with the increase of C-H force constant and charge on the hydrogen atom and with the decrease of C-H bond length [42]. This will cause the conjugation of the oxygen lone pair with the aryl  $p_z$  orbital changes, reaching a maximum when the carbon atom of the methoxy group lies in the plane of the ring ( $\varphi = 0^\circ$ ).

The methoxy asymmetric and symmetric stretch bands are usually observed around  $2960\text{ cm}^{-1}$  and  $2846\text{ cm}^{-1}$  respectively [36-39,43]. DFT computations exhibit three vibrations at  $3016\text{ cm}^{-1}$ ,  $2949\text{ cm}^{-1}$  and  $2892\text{ cm}^{-1}$  respectively. As indicated by the PED, these three modes involve 100%. The asymmetric stretching mode is observed as weak bands at  $2988\text{ cm}^{-1}$  in both IR and Raman spectrum. The asymmetric in phase stretching vibration is active in

IR as a weak band at  $2954\text{ cm}^{-1}$ . The weak band at  $2912\text{ cm}^{-1}$  (Raman) and at  $2912\text{ cm}^{-1}$  (IR) is assigned to methyl symmetric stretching mode. The mode at  $2902\text{ cm}^{-1}$  has 100 %  $\nu_s(\text{CH}_3)$  character. This composition suggests that we can assign confidently this mode to the symmetric stretching of the three methyl C-H bonds.

The asymmetric and symmetric bending vibrations of methyl groups normally appear in the region  $1470\text{-}1440\text{ cm}^{-1}$  and  $1390\text{-}1370\text{ cm}^{-1}$  respectively [36-39]. The weak band at  $1454\text{ cm}^{-1}$  in infrared spectrum and corresponding Raman band at  $1453\text{ cm}^{-1}$  is attributed to the  $\text{CH}_3$  asymmetric bending mode. The weak band around  $1436\text{ cm}^{-1}$  in IR and  $1436\text{ cm}^{-1}$  in Raman spectrum corresponds to the symmetric bending mode. As revealed by the PED, vibrational mode  $\delta\text{CH}_3$  has only 82 % symmetric bending mode. The rocking vibrations of the  $\text{CH}_3$  group in DMBBH appear as mixed vibrations. These modes usually appear in the region  $1170\text{-}1100\text{ cm}^{-1}$  [36-39]. The medium bands observed in IR and Raman spectrum at  $1172\text{ cm}^{-1}$  are attributed to the  $\text{CH}_3$  rocking mode, which is coupled with aromatic CCH bending mode.

The selection allows for C-H attached modes 7b, 2, 20a and 20b for *p*-disubstituted ring [30]. The computed eigen vector distribution using DFT shows that, for *p*-disubstituted ring, mode 20b is found to be active. The weak bands observed at  $3067\text{ cm}^{-1}$  (IR) and at  $3065\text{ cm}^{-1}$  (Raman) is assigned to mode 7b. The normal vibrations 3, 9a, 18a and 15 are classified as C-H in-plane bending

vibrations. The medium band observed at  $1193\text{ cm}^{-1}$  in the IR spectra is assigned to mode 3. The medium bands appearing in both IR and Raman spectrum at  $1152\text{ cm}^{-1}$  corresponds to vibrational mode 9a. The mode 18a is coupled with the C–C stretching mode and is found active in the IR spectrum at  $1104\text{ cm}^{-1}$  as a medium band. Weak band at  $984\text{ cm}^{-1}$  in Raman corresponds to the mode 15. Normal vibration 1 of phenyl ring is usually referred to as substituent sensitive vibration. For heavy substitution the modes found in the region  $900\text{--}800\text{ cm}^{-1}$  are strongly IR active [35]. This is confirmed by the medium band in IR spectra at  $826\text{ cm}^{-1}$ . The C–H out-of-plane bending vibrations are expected in the region  $960\text{--}780\text{ cm}^{-1}$ . The mode 17a is observed in the IR at  $930\text{ cm}^{-1}$ . The weak bands observed in the IR at  $918\text{ cm}^{-1}$  are assigned to 10a mode. The radial skeletal (6a and 6b) and the out-of-plane skeletal (16a and 16b) are listed in Table 3.

The normal modes 8a, 8b, 19a, 19b and 14 are classified as the C–C stretching vibrations. The mode 8a is found at a higher wavenumber than 8b and they appear in the range  $1610\text{--}1580\text{ cm}^{-1}$  [35-39]. According to the calculated PED, the very strong band at  $1600\text{ cm}^{-1}$  in the Raman spectrum is assigned to mode 8, which is described as the in-phase stretching vibrations of the C=C bonds in the aromatic ring  $\nu(\text{C}_{25}\text{--}\text{C}_{26}) + \nu(\text{C}_{22}\text{--}\text{C}_{23})$ . This mode corresponds to the so called mode 8a in the benzene ring [35]. The 8b mode appears as very strong bands at  $1556\text{ cm}^{-1}$  (IR),  $1559\text{ cm}^{-1}$  (solution Raman) and its strong counterpart at  $1558\text{ cm}^{-1}$  in Raman. According to PED calculations, vibrational mode 8b has

only 55 % C–C stretching contribution and 10 % C-H in-plane bending character. The strong band observed at  $1514\text{ cm}^{-1}$  in IR is assigned to the 19a mode and the medium counterpart in the Raman spectrum occurs at  $1514\text{ cm}^{-1}$ . As revealed by the calculated PED, vibrational mode 19a has only 15 % C–C stretching contribution and 47 % C-H in plane bending character. The mode 19b is observed only in the IR spectrum as a weak band at  $1390\text{ cm}^{-1}$ . The 19b mode is attributed to  $1410\text{ cm}^{-1}$ , with significant contribution of, 40 %  $\nu_{\text{CC}}$  and 30 % C-H in plane bending character. The very strong band at  $1279\text{ cm}^{-1}$  in the IR and an intense band at  $1278\text{ cm}^{-1}$  in the Raman spectrum are attributed to vibrational mode 14 of C–C stretching. The 14 mode appears in the calculation at  $1293\text{ cm}^{-1}$  with a composition of 56 % C–C stretch and 28 % C-H in plane bend. The 8b, 19b and 14 modes appear simultaneously in both the IR and Raman spectra providing evidence for charge transfer interaction.

### **5. Molecular Docking Study of DMBH with Phospholipase A<sub>2</sub>**

Based on the Glide energy and Glide score the poses were ranked. The binding mode (figure 1-3) and hydrogen bond interactions (table) were computed. There are six subsites were reported for phospholipase A<sub>2</sub>. Based on the combination of subsites, the target complexes were chosen and subjected for docking with the DMBH. The results confirm that the DMBH prefers the subsite 4, 5 and 6 and is similar to the indomethacin [3] binding mode with human pancreatic secretory PLA<sub>2</sub>. It could be confirmed by the interactions in table 1 and the corresponding

cartoon diagram of the DMBH-PLA<sub>2</sub> complex. In order to confirm the binding preference of DMBH to subsites 4, 5 and 6, the molecular docking is performed with the PLA<sub>2</sub> – inhibitor complexes (monomer and dimer form) with specificity to the subsites 1, 2 and 3. Here, in both the cases, the DMBH failed to interact with the active site amino acids H47 and D48 and shows unfavourable score and energy comparing to the binding with subsites 4, 5 and 6. Hence, the results confirms that DMBH can able to inhibit Phospholipase A2 and exhibit anti-inflammatory and anticoagulant activity thereby indirectly involve in tumor suppression.

## 5. Conclusions

FT-Raman and IR spectra of the Schiff base compound, 2,4-dihydroxy-*N'*-(methoxybenzylidene) benzohydrazide have been recorded and analyzed. The detailed interpretation of the vibrational spectra has been carried out with the aid of normal coordinate analysis (NCA) following the scaled quantum mechanical force field methodology. The various intramolecular interactions that is responsible for the stabilization of the molecule was revealed by natural bond orbital analysis. Information about the size, shape, charge density distribution and site of chemical reactivity of the molecules has been obtained by mapping electron density isosurface with electrostatic potential surfaces (ESP). A complete vibrational analysis has been attempted on the basis of experimental infrared and Raman spectra, calculated frequency, intensity of the vibrational

bands and potential energy distribution over the internal coordinates. The broadening of the band at about  $1631\text{ cm}^{-1}$  and the appearance of the band at  $1556\text{ cm}^{-1}$  strongly suggests the existence of proton equilibrium. The lowering of HOMO and LUMO energy gap clearly explicates the charge transfer interactions taking place within the molecule.

### **Acknowledgements**

The financial support within the frame of long term research plan of the Ministry of Education of the Czech Republic No. MSM0021620857 is gratefully acknowledged (I.N.).

### **References**

- [1] P.G. Cozzi, Metal–Salen Schiff base complexes in catalysis: practical aspects, *Chem.Soc.Rev.*33 (2004) 410-421.

- [2] W.P Jencks, *Catalysis in Chemistry and Enzymology*. McGraw-Hill, New York, 1997.
- [3] C. Desfranc, ois, S. Carles, J.P. Schermann, Weakly bound clusters of biological interest, *Chem. Rev.* 100 (2000) 3943–3962.
- [4] E. Hadjoudis, M.Vittorakis, I.Moustakali-Mavridis, Photochromism and thermochromism of schiff bases in the solid state and in rigid glasses ,*Tetrahedron* 43 (1987)1345.
- [5] S. Perun, A.L. Sobolewski, W. Domcke, Role of electron-driven proton-transfer processes in the excited-state deactivation of the adenine–thymine base pair, *J. Phys. Chem. A* 110 (2006) 9031–9038.
- [6] J.M. Fernández-G, F.del reio-Portilla, B.Quiroz-Garcia, R.A.Toscano, R.Salcedo, The synthesis, X-ray and DFT structures of the free ansa–cyclopentadiene ligand  $C_5H_5CMe_2CMe_2C_5H_5$  , *J.Mol.Struct.*561 (2001)197.
- [7] M.Kabak, A.Elimali, Y.Elerman, T.N.Durlu, Conformational study and structure of bis-*N,N'*-*p*-bromo-salicylideneamine-1,2-diaminobenzene, *J.Mol.Struct.*553 (2000) 187.
- [8]. S.Arulmurugan<sup>1</sup>, Helen P. Kavitha<sup>1</sup> and B.R. Venkatraman , *Biological Activities of Schiff Bases and its complexes : A Review* , *Rasayan J.Chem.*3 (2010) 385-410.

[9] J.Costamagna, J.Vargas, R.Lattore, A.Alvarado, G.Mena, Coordination compounds of copper, nickel and iron with Schiff bases derived from hydroxynaphthaldehydes and salicylaldehydes, *Coord. Chem. Rev.*119 (1992) 67-88.

[10] Yun-Peng Diao, Shan-Shan Huang, Jian-Kui Zhang and Ting-Guo Kang, 2,4-Dihydroxy-N'-(4-methoxybenzylidene)benzohydrazide, *Acta Cryst.* (2008). E64, o470.

[11] D. Sajan, K. P Laladhas, I. Hubert Joe and V.S. Jayakumar, Vibrational spectra and density functional theoretical calculations on the antitumor drug, plumbagin, *J. Raman Spectrosc.*36 (2005) 1001-1011.

[12] D. Sajan, G. D. Sockalingum, M. Manfait, I. Hubert Joe and V. S. Jayakumar, NIR-FT Raman, FT-IR and surface-enhanced Raman scattering spectra, with theoretical simulations on chloramphenicol *J. Raman Spectrosc.* 39 (2008) 1772-1783.

[13]D. Sajan, J. Binoy, B. Pradeep, K. Venkata Krishna, V.B. Kartha, I. Hubert Joe, V.S.

Jayakumar, NIR-FT Raman and infrared spectra and *ab initio* computations of glycinium oxalate, *Spectrochim. Acta A* 60 (2004) 173-180.

[14] J. Binoy, Jose P. Abraham, I. Hubert Joe, V.S. Jayakumar, G.R. Pettit and O.F. Nielsen, NIR-FT Raman and FT-IR spectral studies and *ab initio*

calculations of the anti-cancer drug combretastatin-A4, *J. Raman Spectrosc.* 35 (2004) 939-946.

[15] D. Sajan, I.H. Joe, J. Zaleski, V.S. Jayakumar, Structural and electronic contributions to hyperpolarizability in methyl *p*-hydroxy benzoate, *J. Mol. Struct.* 785 (2006) 43-53.

[16] D. Sajan, I. Hubert Joe and V.S. Jayakumar, NIR-FT Raman, FT-IR and surface-enhanced Raman scattering spectra of organic nonlinear optic material: *p*-hydroxy acetophenone, *J. Raman Spectrosc.* 37 (2006) 508-519.

[17] D. Sajan, H.J. Ravindra, Neeraj Misra, I. Hubert Joe, Intramolecular charge transfer and hydrogen bonding interactions of nonlinear optical material *N*-benzoyl glycine: Vibrational spectral study, *Vibrational Spectroscopy* 54 (2010) 72-80.

[18] Omnic version 7.4, Thermo Fisher Scientific Inc., Madison, USA, 2007.

[19]. M. J. Frisch, G. W. Trucks, H. B. Schlegel, G. E. Scuseria, M. A. Robb, J. R. Cheeseman, J. A. Montgomery Jr, T. Vreven, K. N. Kudin, J. C. Burant, J. M. Millam, S. S. Iyengar, J. Tomasi, V. Barone, B. Mennucci, M. Cossi, G. Scalmani, N. Rega, G. A. Petersson, H. Nakatsuji, M. Hada, M. Ehara, K. Toyota, R. Fukuda, J. Hasegawa, M. Ishida, T. Nakajima, Y. Honda, O. Kitao, H. Nakai, M. Klene, X. Li, J. E. Knox, H. P. Hratchian, J. B. Cross, V. Bakken, C. Adamo, J. Jaramillo, R. Gomperts, R. E. Stratmann, O. Yazyev, A. J. Austin, R. Cammi, C. Pomelli, J. W. Ochterski, P. Y. Ayala, K. Morokuma, G. A. Voth, P. Salvador, J. J. Dannenberg, V.

G Zakrzewski, S Dapprich, A. D Daniels, M. C Strain, O Farkas, D. K Malick, A. D Rabuck, K Raghavachari, J. B Foresman, J. V Ortiz, Q Cui, A. G Baboul, S Clifford, J Cioslowski, B. B Stefanov, G Liu, A Liashenko, P Piskorz, I Komaromi, R. L Martin, D. J Fox, T Keith, M. A Al-Laham, C. Y Peng, A Nanayakkara, M Challacombe, P. MW Gill, B Johnson, W Chen, M.W Wong, C Gonzalez, J. A Pople, Gaussian 03, Revision D01, Gaussian: Wallingford, 2004.

[20] A.D. Becke, Density functional thermochemistry. III. The role of exact exchange, *J. Chem. Phys.* 98 (1999) 5648-5652.

[21] M.H. Jamróz, Vibrational energy distribution analysis VEDA 4, Warsaw, 2004.

[22] A.P. Scott, L. Radom, Harmonic Vibrational Frequencies: An Evaluation of Hartree–Fock, Møller–Plesset, Quadratic Configuration Interaction, Density Functional Theory, and Semiempirical Scale Factors, *J. Phys. Chem.* 100 (1996) 16502-16513.

[23] G. Keresztury, S. Holly, J. Varga, G. Besenyi, A.Y. Wang, J.R. Durig, Vibrational spectra of monothiocarbamates-II. IR and Raman spectra, vibrational assignment, conformational analysis and *ab initio* calculations of *S*-methyl-*N,N*-dimethylthiocarbamate *Spectrochim. Acta A* 49 (1993) 2007-2017.

[24] E.D. Glendening, J. K. Badenhoop, A. E. Reed, J. E. Carpenter, J. A. Bohmann, C. M. Morales, F. Weinhold, NBO 5.0, Theoretical Chemistry Institute, University of Wisconsin: Madison, 2001

- [25] F. Weinhold, Chemistry: A new twist on molecular shape, Nature 411 (2001) 539-541.
- [26] F. Weinhold, C. Landis, Valency and Bonding: A Natural Bond Orbital Donor–Acceptor Perspective, Cambridge University Press: Cambridge, 2005.
- [27] M. Odabasoglu, C. Albayrak, O. Buyukgnugor, P. Lonneck, 2-[[Tris(hydroxymethyl)methyl]aminomethylene]cyclohexa-3,5-dien-1(2*H*)-one and its 6-hydroxy and 6-methoxy derivatives, Acta Cryst. C59 (2003). 616-619.
- [28] P. Gilli, F. Belluci, V. Ferretti, V. Bertolasi, Evidence for resonance-assisted hydrogen bonding from crystal-structure correlations on the enol form of the .beta.-diketone fragment, J. Am. Chem. Soc. 111(1989)1023-1028.
- [29] A. Filarowski, Intramolecular hydrogen bonding in *o*-hydroxyaryl Schiff bases, J. Phys. Org. Chem. 18(2005) 686-698.
- [30] U.C. Singh and P.A. Kollman, An approach to computing electrostatic charges for molecules, J. Comput. Chem. 5 (1984) 129-145.
- [31] M.L. Connolly, Solvent-Accessible Surfaces of Proteins and Nucleic Acids Science 221 (1983) 709-713.
- [32] P. Sjoberg, J.S. Murray, T. Brinck and P. Politzer, Average local ionization energies on the molecular surfaces of aromatic systems as guides to chemical reactivity, Can. J. Chem. 68 (1990) 1440-1443.

- [33] J.S. Murray and P. Politzer In: C. Párkányi, Editor, Theoretical Organic Chemistry. Theoretical and Computational Chemistry vol. 5, Elsevier, Amsterdam (1998) 189.
- [34] Ralf Stowasser and Roald Hoffmann, What Do the Kohn–Sham Orbitals and Eigenvalues Mean, J. Am. Chem. Soc. 121 (1999) 3414-3420.
- [35] G. Varsanyi, Vibrational Spectra of Benzene Derivatives, Academic Press, New York, 1969.
- [36] B. Smith Infrared Spectral Interpretation, A Systematic Approach. CRC Press: Washington, DC, 1999
- [37] N.B. Colthup, L.H. Daly, S.E. Wiberley Introduction to Infrared and Raman Spectroscopy. Academic Press: New York, 1990.
- [38] F.R. Dollish, W.G. Fateley, F.F. Bentley, Characteristic Raman Frequencies of Organic Compounds, John Wiley & Sons, New York, 1997
- [39] L.J. Bellamy, The Infra-red Spectra of Complex Molecules, John Wiley and Sons Inc., New York, 1975
- [40] O. Poizat, V. Guichary, Vibrational studies of reactive intermediates of aromatic amines. IV. Radical cation time-resolved resonance Raman investigation of *N*, *N*-dimethylaniline and *N*, *N*-diethylaniline derivatives J. Chem. Phys. 90 (1989) 4697-4703.

[41] H. Okamoto, H. Inishi, Y. Nakamura, S. Kohtani, R. Nakagaki, Infrared and Raman spectra of 4-(dimethylamino)benzotrile and isotopomers in the ground state and vibrational analysis ,Chem. Phys. 260 (2000) 193-214.

[42] M. Gussoni, C. Castiglioni, J. Mol.Struct. Infrared intensities. Use of the CH-stretching band intensity as a tool for evaluating the acidity of hydrogen atoms in hydrocarbons, 521 (2000)1-18.

[43] G. Socrates, Infrared Characteristic Group Frequencies, John Wiley and Sons, Ltd., New York, 1980.

**Figure Caption**

Fig. 1 Optimized molecular structure of DMBBH (a) Cis (b) Trans

Fig. 2 Potential energy surface scan for dihedral angles  $C_1-C_{14}-N_{16}-N_{18}$

Fig. 3 Potential energy surface scan for dihedral angles  $C_{25}-C_{24}-O_{31}-C_{32}$

Fig. 4 Potential energy surface scan for torsion around O-H group (a)  $C_5-C_4-O_9-H_{10}$  (b)  $C_5-C_6-O_7-H_{13}$

Fig. 5. The Mulliken charge distribution of DMBBH calculated at the B3LYP/6-31G(d) level of theory

Fig. 6. HOMO and LUMO plot of DMBBH at B3LYP/6-31G(d).

Figure-7 Electron density isosurface mapped with Electrostatic potential surface for DMBBH calculated at B3LYP/6-31G(d) levels of theory (a) Electrostatic

potential surface ,(b) Electrostatic potential counter map, (c) local ionization potential and (d) Total density

Fig. 8. FT-IR and simulated IR spectra of DMBBH

Fig. 9. FT-Raman and simulated Raman spectra of DMBBH

ACCEPTED MANUSCRIPT

Table Caption

Table 1 Second order perturbation theory analysis of Fock matrix in NBO basis

Table 2 Optimized Geometry of DMBHH Cis and Trans conformation by  
B3LYP/6-31G(d) in comparison with XRD data

Table-3. Calculated vibrational wavenumbers, measured IR and Raman band  
positions ( $\text{cm}^{-1}$ ) and assignments for DMBBH

ACCEPTED MANUSCRIPT

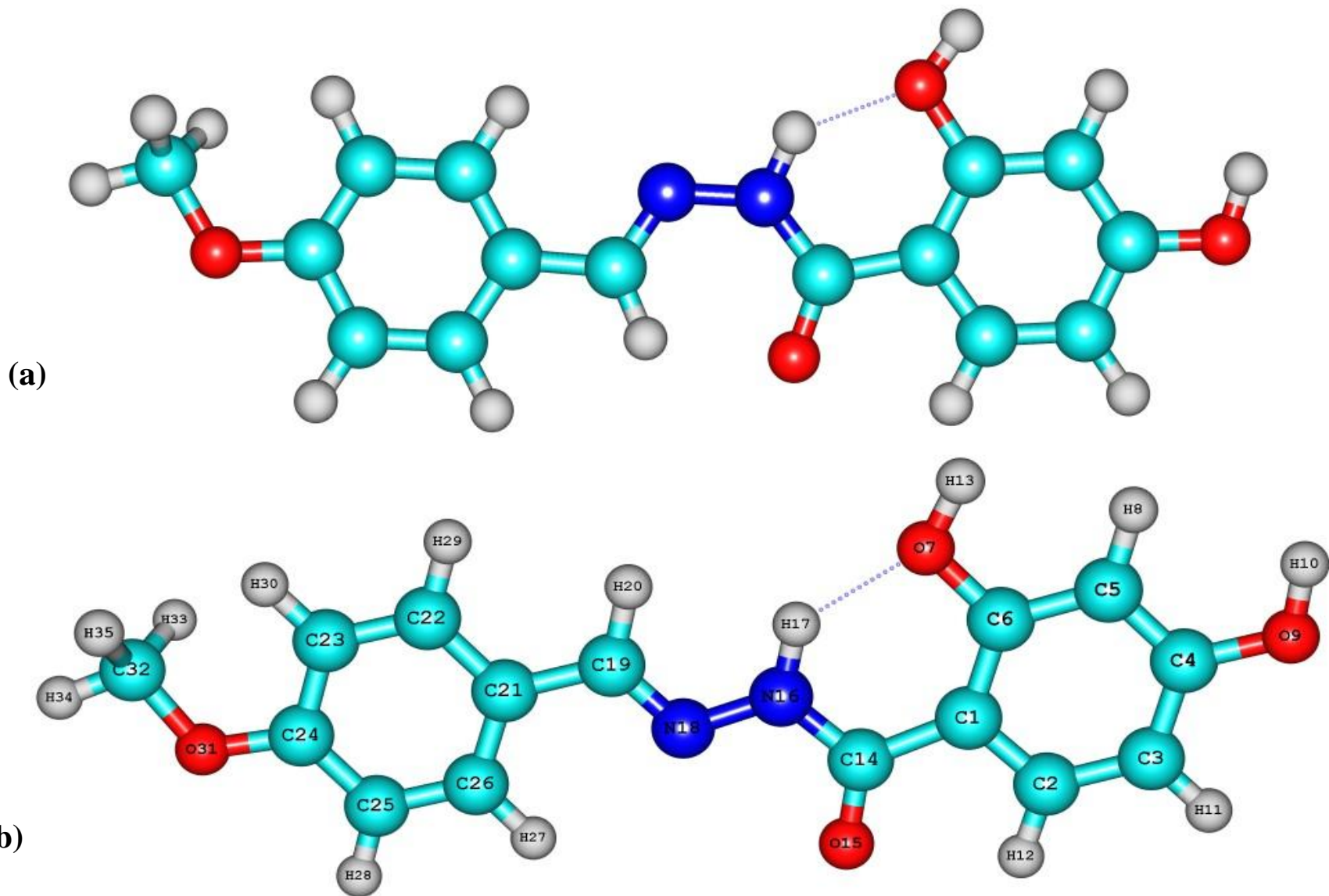


Fig. 1 Optimized molecular structure of DMBBH (a) Cis (b) Trans

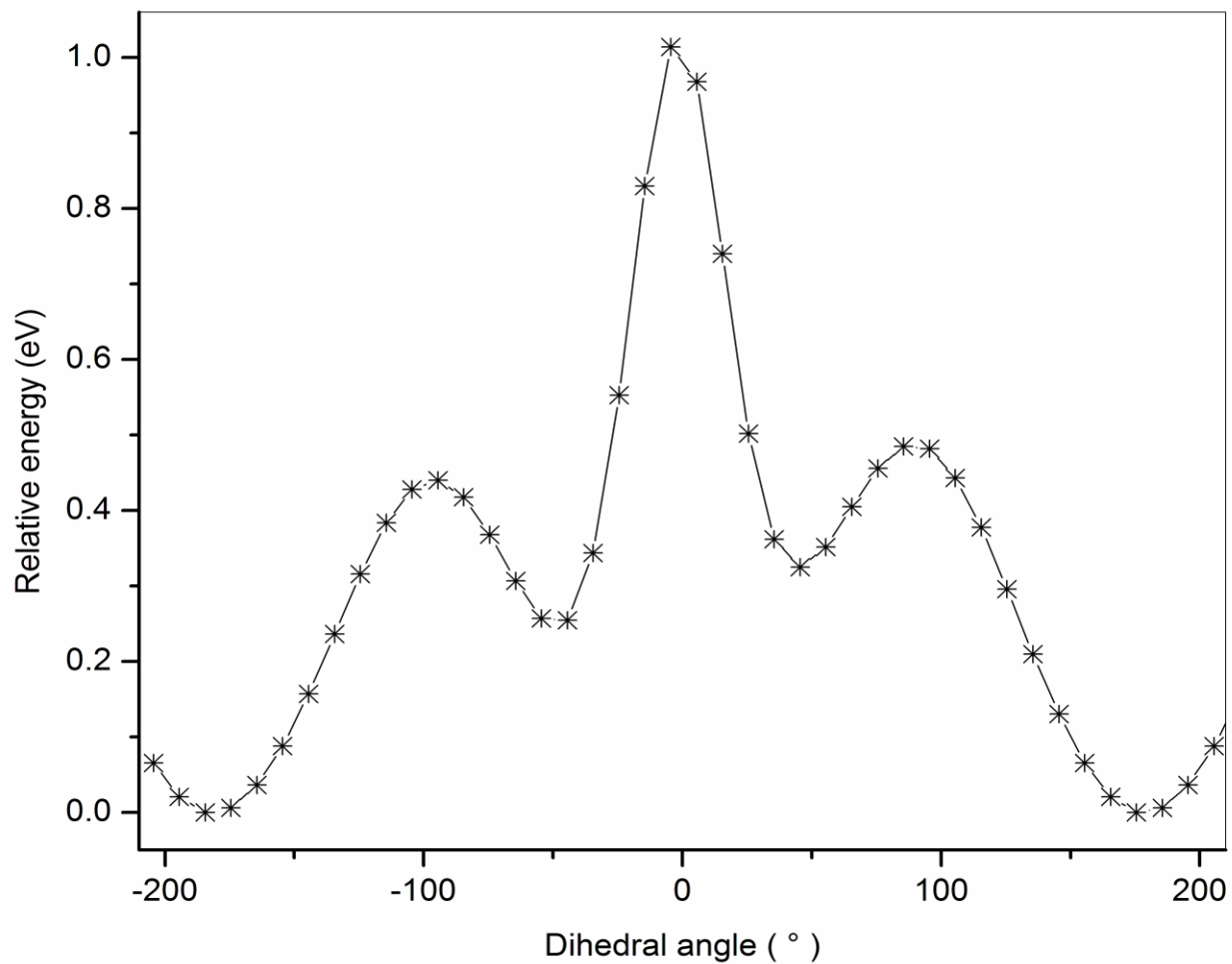
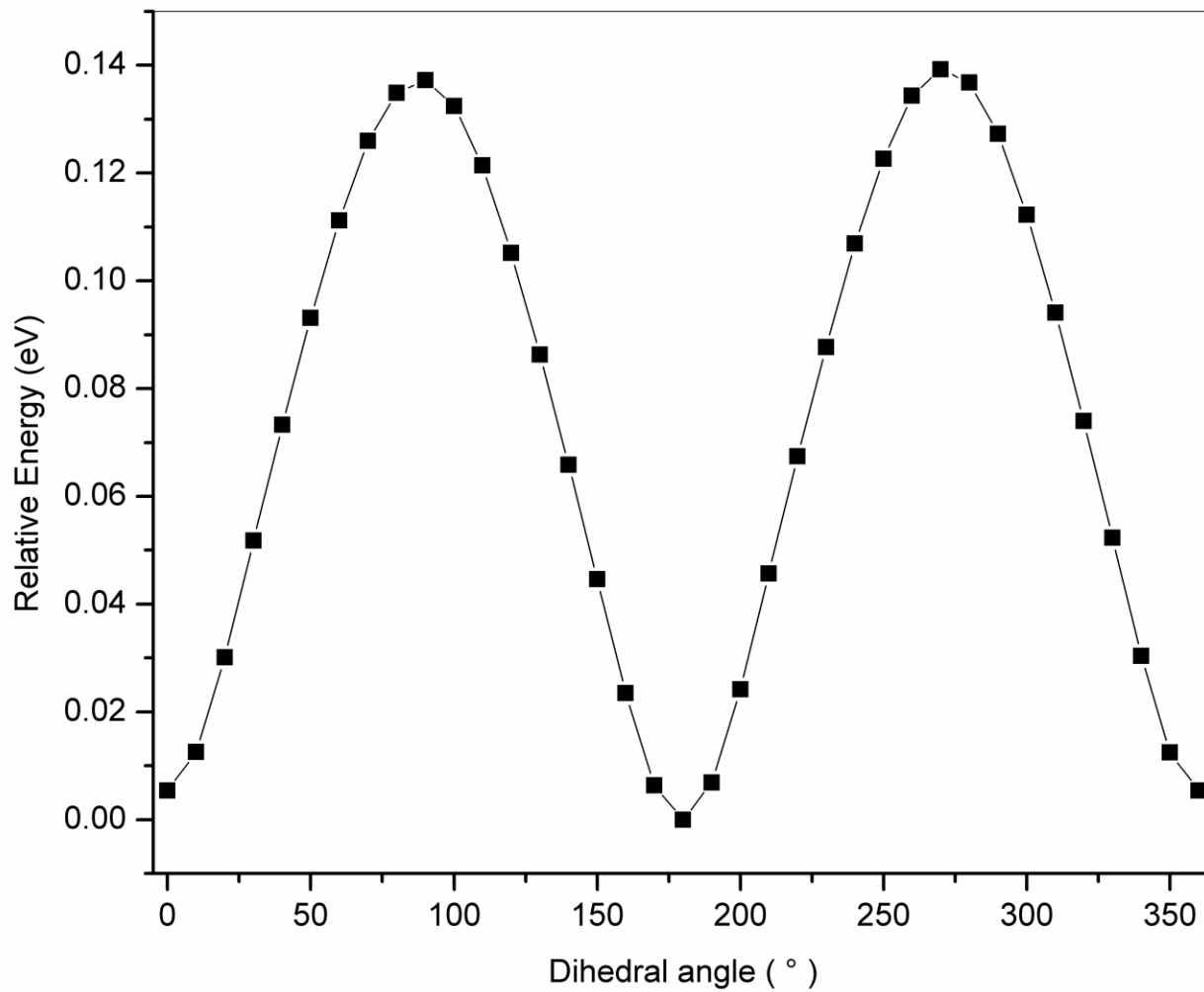
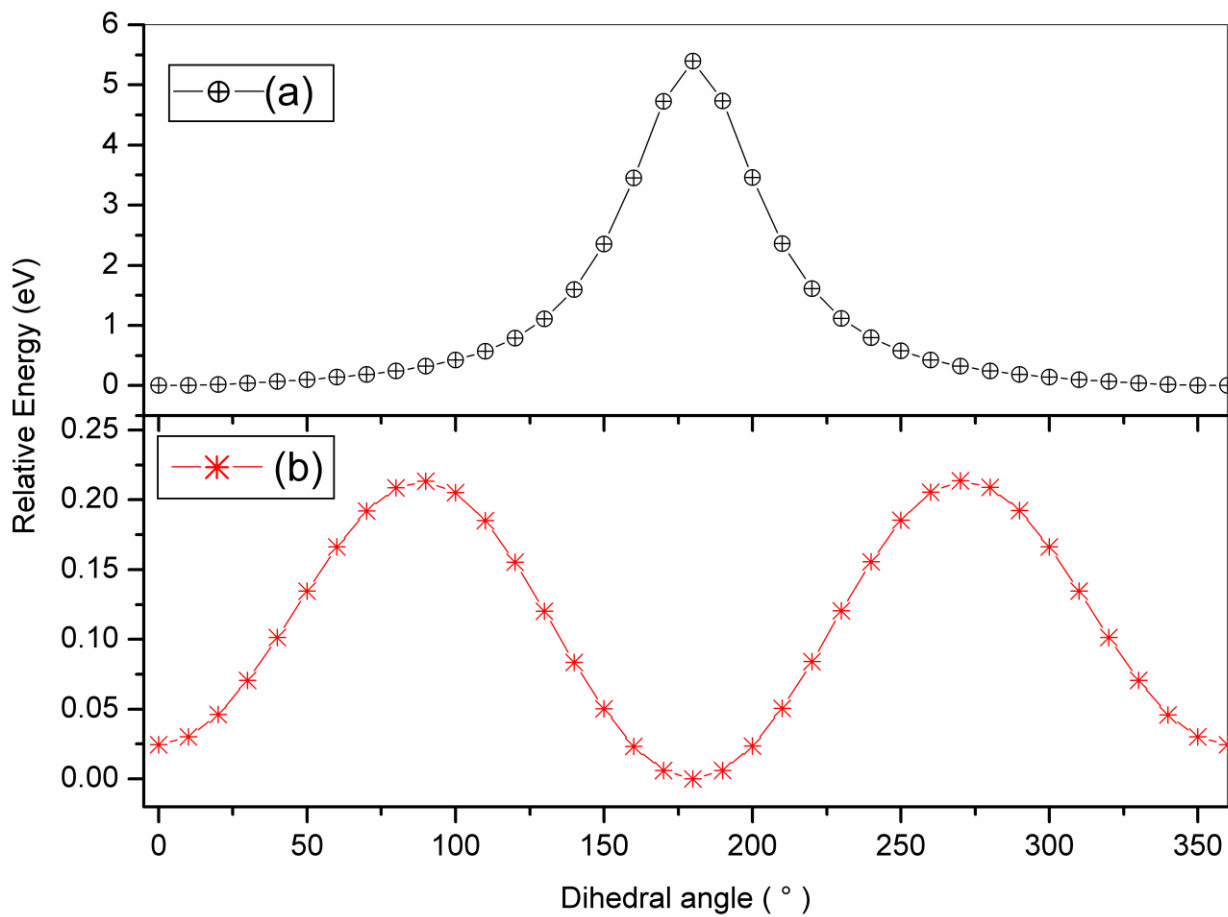


Fig. 2 Potential energy surface scan for dihedral angles C<sub>1</sub>-C<sub>14</sub>-N<sub>16</sub>-N<sub>18</sub>



**Fig. 3** Potential energy surface scan for dihedral angles  $C_{25}-C_{24}-O_{31}-C_{32}$



**Fig. 4** Potential energy surface scan for torsion around O-H group (a) C<sub>5</sub>-C<sub>4</sub>-O<sub>9</sub>-H<sub>10</sub> (b) C<sub>5</sub>-C<sub>6</sub>-O<sub>7</sub>-H<sub>13</sub>

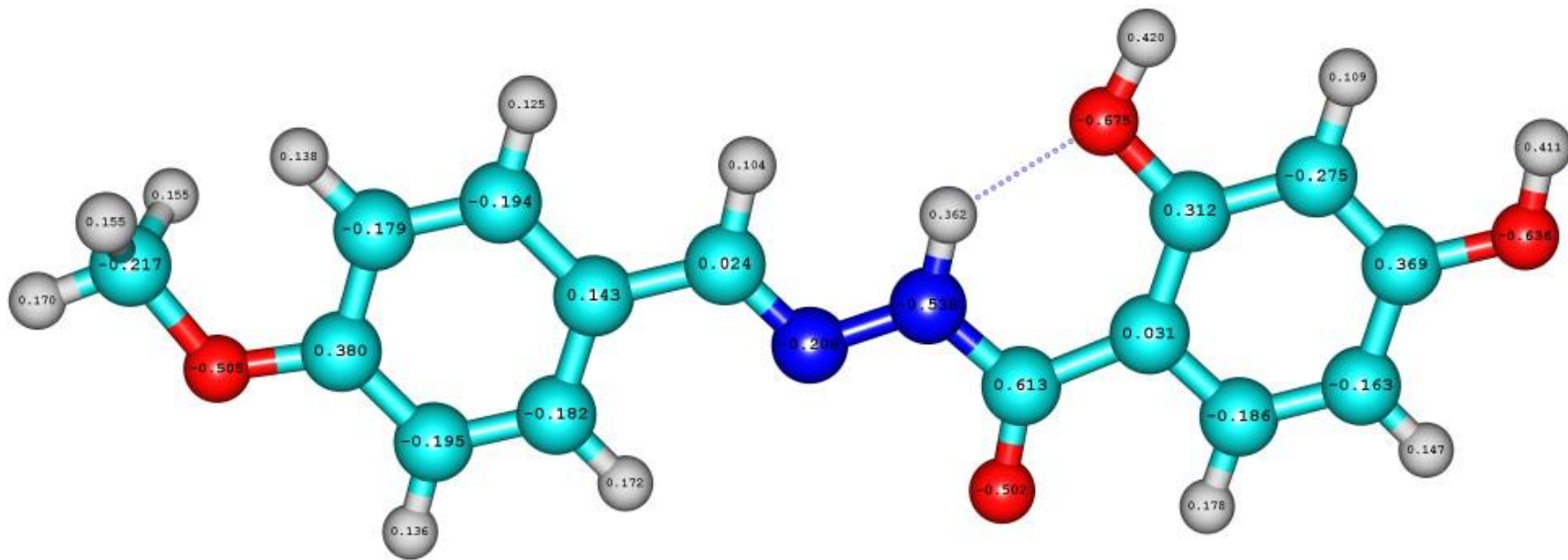


**Fig. 5.** The Mulliken charge distribution of DMBBH calculated at the B3LYP/6-31G(d) level of theory

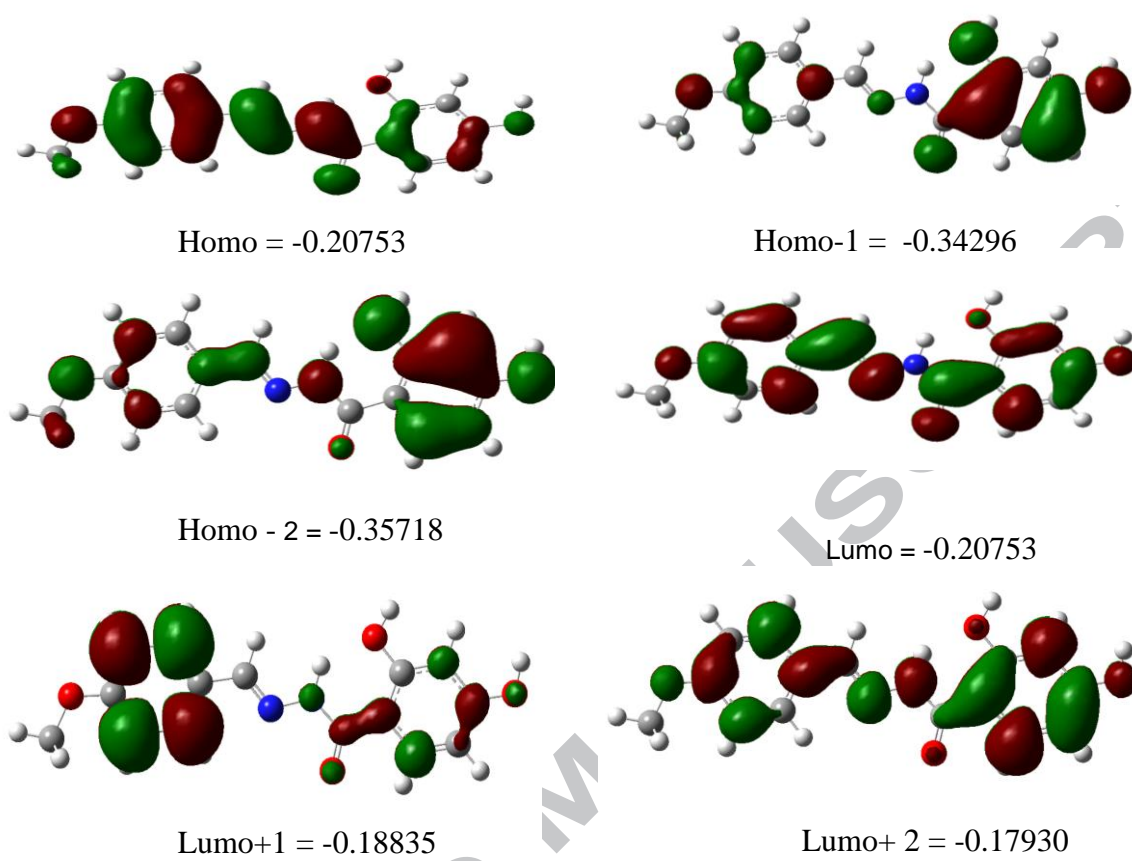
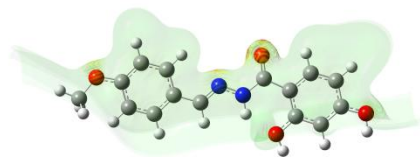
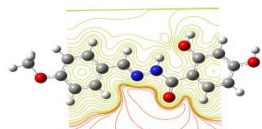


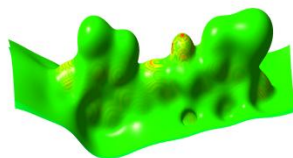
Fig. 6. HOMO and LUMO plot of DMBBH at B3LYP/6-31G(d).



(a)



(b)



(c)



(d)

Figure-7 Electron density isosurface mapped with Electrostatic potential surface for DMBBH calculated at B3LYP/6-31G(d) levels of theory (a) Electrostatic potential surface ,(b) Electrostatic potential counter map, (c) local ionization potential and (d) Total density

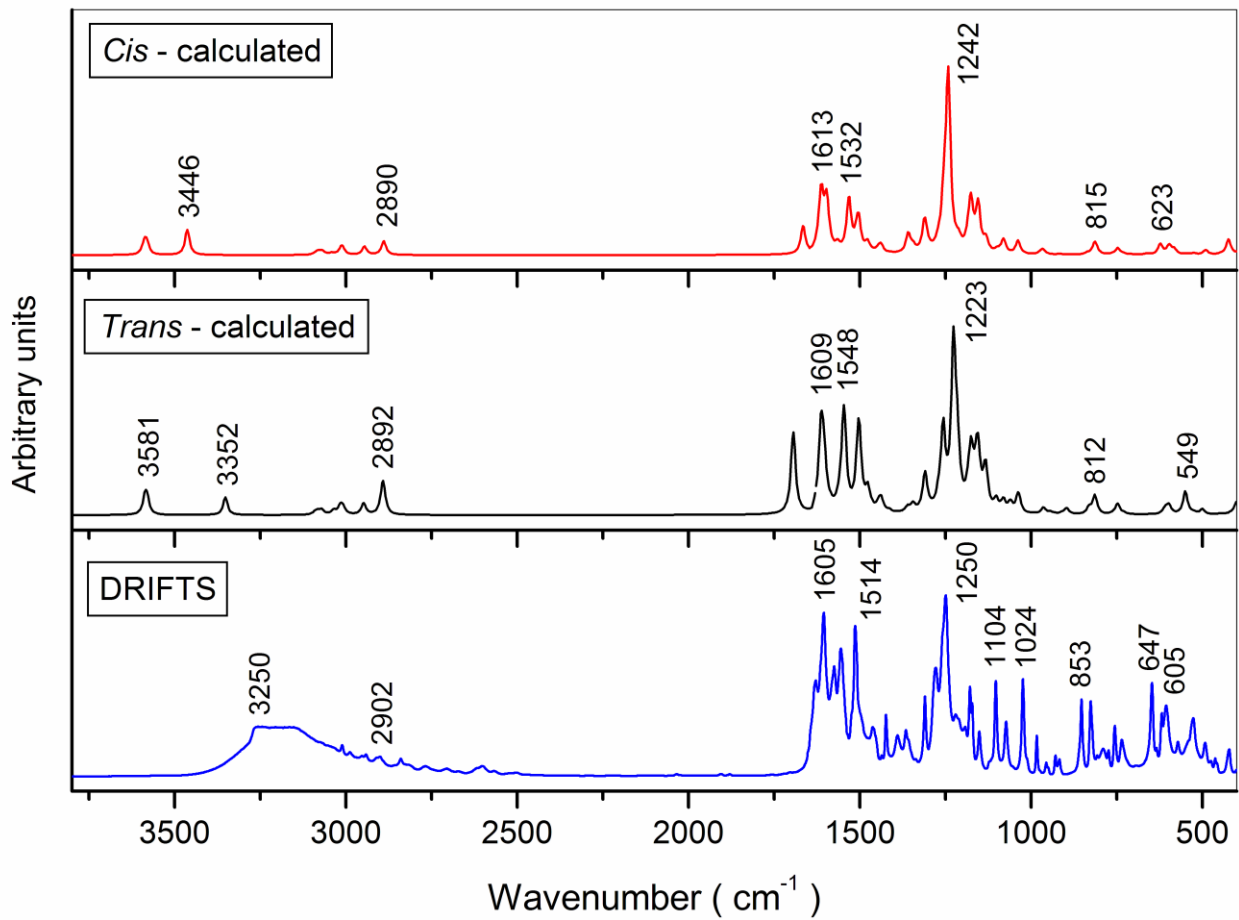
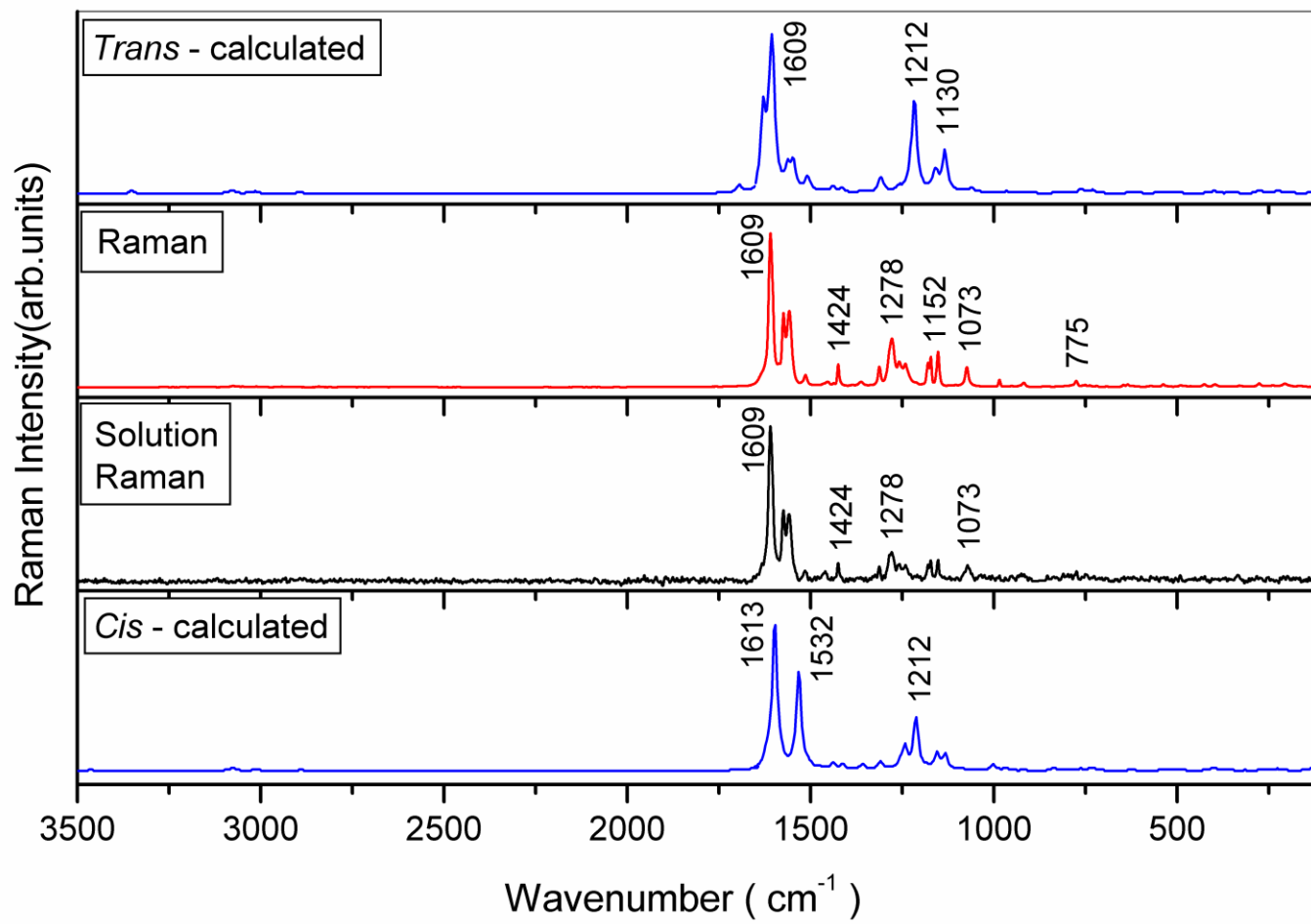


Fig. 8. FT-IR and simulated IR spectra of DMBBH



**Fig. 9.** FT-Raman and simulated Raman spectra of DMBBH

Table 1 Second order perturbation theory analysis of Fock matrix in NBO basis

Lone pair	Occupancy	Donor– acceptor interaction	$E(2)^a$ (KJ mol <sup>-1</sup> )	$E(j)-E(i)^b$ (a.u.)	$F(i,j)^c$ (a.u.)
LP <sub>1</sub> O <sub>7</sub>	1.9650	$n$ (LP <sub>1</sub> O <sub>7</sub> ) → $\sigma^*$ (C <sub>5</sub> -C <sub>6</sub> )	21.34	1.17	0.069
		$n$ (LP <sub>1</sub> O <sub>7</sub> ) → $\sigma^*$ (N <sub>16</sub> -H <sub>17</sub> )	37.45	1.07	0.088
LP <sub>2</sub> O <sub>7</sub>	1.8831	$n$ (LP <sub>2</sub> O <sub>7</sub> ) → $\pi^*$ (C <sub>1</sub> -C <sub>6</sub> )	109.1	0.37	0.095
LP <sub>1</sub> O <sub>9</sub>	1.9793	$n$ (LP <sub>1</sub> O <sub>9</sub> ) → $\sigma^*$ (C <sub>4</sub> -C <sub>5</sub> )	26.99	1.16	0.077
LP <sub>2</sub> O <sub>9</sub>	1.8631	$n$ (LP <sub>2</sub> O <sub>9</sub> ) → $\pi^*$ (C <sub>4</sub> -C <sub>5</sub> )	132.6	0.34	0.10
LP <sub>1</sub> O <sub>15</sub>	1.9779	$n$ (LP <sub>1</sub> O <sub>15</sub> ) → $\sigma^*$ (C <sub>4</sub> -C <sub>14</sub> )	11.34	1.08	0.049
		$n$ (LP <sub>1</sub> O <sub>15</sub> ) → $\sigma^*$ (C <sub>14</sub> -N <sub>16</sub> )	5.81	1.12	0.036
LP <sub>2</sub> O <sub>15</sub>	1.8535	$n$ (LP <sub>2</sub> O <sub>15</sub> ) → $\sigma^*$ (C <sub>4</sub> -C <sub>14</sub> )	85.77	0.65	0.105
		$n$ (LP <sub>2</sub> O <sub>15</sub> ) → $\sigma^*$ (C <sub>2</sub> -H <sub>12</sub> )	3.80	0.72	0.024
		$n$ (LP <sub>2</sub> O <sub>15</sub> ) → $\sigma^*$ (C <sub>14</sub> -N <sub>16</sub> )	116.3	0.68	0.125
LP <sub>1</sub> N <sub>16</sub>	1.6522	$n$ (LP <sub>2</sub> N <sub>16</sub> ) → $\pi^*$ (C <sub>14</sub> -O <sub>15</sub> )	243.1	0.29	0.116
		$n$ (LP <sub>2</sub> N <sub>16</sub> ) → $\pi^*$ (N <sub>18</sub> -C <sub>19</sub> )	121.1	0.28	0.083
LP <sub>1</sub> N <sub>18</sub>	1.9212	$n$ (LP <sub>2</sub> N <sub>18</sub> ) → $\sigma^*$ (N <sub>16</sub> -H <sub>17</sub> )	34.27	0.81	0.073
		$n$ (LP <sub>2</sub> N <sub>18</sub> ) → $\sigma^*$ (C <sub>19</sub> -H <sub>20</sub> )	45.81	0.79	0.084
		$n$ (LP <sub>2</sub> N <sub>18</sub> ) → $\sigma^*$ (C <sub>19</sub> -C <sub>21</sub> )	8.20	0.87	0.037
LP <sub>1</sub> O <sub>31</sub>	1.9637	$n$ (LP <sub>1</sub> O <sub>31</sub> ) → $\sigma^*$ (C <sub>23</sub> -C <sub>24</sub> )	2.76	1.11	0.024
		$n$ (LP <sub>1</sub> O <sub>31</sub> ) → $\sigma^*$ (C <sub>24</sub> -C <sub>25</sub> )	31.25	1.10	0.081
		$n$ (LP <sub>1</sub> O <sub>31</sub> ) → $\sigma^*$ (C <sub>32</sub> -H <sub>33</sub> )	5.18	0.97	0.031
		$n$ (LP <sub>1</sub> O <sub>31</sub> ) → $\sigma^*$ (C <sub>32</sub> -H <sub>34</sub> )	7.74	1.00	0.039
		$n$ (LP <sub>1</sub> O <sub>31</sub> ) → $\sigma^*$ (C <sub>32</sub> -H <sub>35</sub> )	5.18	0.97	0.031
LP <sub>2</sub> O <sub>31</sub>	1.8355	$n$ (LP <sub>2</sub> O <sub>31</sub> ) → $\pi^*$ (C <sub>23</sub> -C <sub>25</sub> )	129.3	0.34	0.097
		$n$ (LP <sub>2</sub> O <sub>31</sub> ) → $\sigma^*$ (C <sub>32</sub> -H <sub>33</sub> )	22.8	0.73	0.059
		$n$ (LP <sub>2</sub> O <sub>31</sub> ) → $\sigma^*$ (C <sub>32</sub> -H <sub>35</sub> )	22.8	0.73	0.059

Table 2 Optimized Geometry of DMBHH Cis and Trans conformation by B3LYP/6-31G(d) in comparison with XRD data

Bond Length	Cis	Trans	X-ray	Bond Angle	Cis	Trans	X-ray	Torsion angle	Cis	Trans	X-ray
C <sub>1</sub> -C <sub>2</sub>	1.406	1.406	1.394	C <sub>1</sub> -C <sub>2</sub> -C <sub>3</sub>	123.02	123.04	122.94	C <sub>1</sub> -C <sub>2</sub> -C <sub>3</sub> -C <sub>4</sub>	0.001	0.0	-1.3
C <sub>2</sub> -C <sub>3</sub>	1.384	1.384	1.375	C <sub>2</sub> -C <sub>3</sub> -C <sub>4</sub>	118.96	118.97	118.52	C <sub>2</sub> -C <sub>3</sub> -C <sub>4</sub> -C <sub>5</sub>	0.000	0.0	2.5
C <sub>3</sub> -C <sub>4</sub>	1.399	1.399	1.393	C <sub>3</sub> -C <sub>4</sub> -C <sub>5</sub>	119.87	119.84	120.36	C <sub>3</sub> -C <sub>4</sub> -C <sub>5</sub> -C <sub>6</sub>	-0.001	0.0	-0.8
C <sub>4</sub> -C <sub>5</sub>	1.396	1.396	1.380	C <sub>4</sub> -C <sub>5</sub> -C <sub>6</sub>	120.25	120.23	120.26	C <sub>4</sub> -C <sub>5</sub> -C <sub>6</sub> -C <sub>1</sub>	0.000	0.0	-2.2
C <sub>5</sub> -C <sub>6</sub>	1.397	1.397	1.384	C <sub>5</sub> -C <sub>6</sub> -C <sub>1</sub>	121.12	121.19	120.82	C <sub>5</sub> -C <sub>6</sub> -C <sub>1</sub> -C <sub>2</sub>	0.001	0.0	3.4
C <sub>6</sub> -C <sub>1</sub>	1.408	1.408	1.405	C <sub>6</sub> -C <sub>1</sub> -C <sub>2</sub>	116.79	116.73	117.00	C <sub>6</sub> -C <sub>1</sub> -C <sub>2</sub> -C <sub>3</sub>	-0.001	0.0	-1.7
C <sub>2</sub> -H <sub>12</sub>	1.084	1.084	0.930	C <sub>1</sub> -C <sub>2</sub> -H <sub>12</sub>	116.45	116.30	118.50	C <sub>6</sub> -C <sub>1</sub> -C <sub>2</sub> -H <sub>12</sub>	179.99	-180.0	178.3
C <sub>3</sub> -H <sub>11</sub>	1.084	1.084	0.931	C <sub>2</sub> -C <sub>3</sub> -H <sub>11</sub>	121.72	121.71	120.80	C <sub>1</sub> -C <sub>2</sub> -C <sub>3</sub> -H <sub>11</sub>	-179.99	-180.0	178.7
C <sub>4</sub> -O <sub>9</sub>	1.361	1.362	1.365	C <sub>3</sub> -C <sub>4</sub> -O <sub>9</sub>	117.69	117.68	117.50	C <sub>6</sub> -C <sub>5</sub> -C <sub>4</sub> -O <sub>9</sub>	-180.00	180.0	179.2
O <sub>9</sub> -H <sub>10</sub>	0.969	0.969	0.820	C <sub>4</sub> -O <sub>9</sub> -H <sub>10</sub>	109.58	109.59	109.50	C <sub>5</sub> -C <sub>4</sub> -O <sub>9</sub> -H <sub>10</sub>	-0.01	0.0	-0.90
C <sub>5</sub> -H <sub>8</sub>	1.090	1.090	0.930	C <sub>4</sub> -C <sub>5</sub> -H <sub>8</sub>	120.15	120.16	119.90	C <sub>1</sub> -C <sub>6</sub> -C <sub>5</sub> -H <sub>8</sub>	-179.99	-180.0	177.8
C <sub>6</sub> -O <sub>7</sub>	1.374	1.376	1.366	C <sub>5</sub> -C <sub>6</sub> -O <sub>7</sub>	119.58	119.37	119.10	C <sub>4</sub> -C <sub>5</sub> -C <sub>6</sub> -O <sub>7</sub>	179.99	180.0	179.5
O <sub>7</sub> -H <sub>13</sub>	0.969	0.969	0.820	C <sub>6</sub> -O <sub>7</sub> -H <sub>13</sub>	109.85	109.58	109.50	C <sub>5</sub> -C <sub>6</sub> -O <sub>7</sub> -H <sub>13</sub>	.024	0.005	-25.8
C <sub>1</sub> -C <sub>14</sub>	1.507	1.507	1.483	C <sub>1</sub> -C <sub>14</sub> -O <sub>15</sub>	120.32	121.01	121.91	C <sub>6</sub> -C <sub>1</sub> -C <sub>14</sub> -O <sub>15</sub>	-179.99	-180.0	179.2
C <sub>14</sub> -O <sub>15</sub>	1.231	1.222	1.235	C <sub>14</sub> -N <sub>16</sub> -H <sub>17</sub>	117.98	119.62	120.00	C <sub>1</sub> -C <sub>14</sub> -N <sub>16</sub> -H <sub>17</sub>	-0.004	-0.001	0.4
C <sub>14</sub> -N <sub>16</sub>	1.374	1.382	1.340	N <sub>16</sub> -N <sub>18</sub> -C <sub>19</sub>	121.56	116.83	114.96	C <sub>14</sub> -N <sub>16</sub> -N <sub>18</sub> -C <sub>19</sub>	0.012	180.0	175.9
N <sub>16</sub> -H <sub>17</sub>	1.010	1.017	0.90	N <sub>18</sub> -C <sub>19</sub> -H <sub>20</sub>	122.55	121.47	118.10	N <sub>16</sub> -N <sub>18</sub> -C <sub>19</sub> -H <sub>20</sub>	0.000	0.0	-1.5
N <sub>16</sub> -N <sub>18</sub>	1.371	1.358	1.379	C <sub>21</sub> -C <sub>19</sub> -H <sub>20</sub>	117.61	116.52	118.20	H <sub>20</sub> -C <sub>19</sub> -C <sub>21</sub> -C <sub>22</sub>	0.011	0.0	-0.5
N <sub>18</sub> -C <sub>19</sub>	1.290	1.285	1.270	C <sub>19</sub> -C <sub>21</sub> -C <sub>22</sub>	119.03	119.84	121.10	C <sub>19</sub> -C <sub>21</sub> -C <sub>22</sub> -C <sub>23</sub>	179.99	-180.0	-179.7
C <sub>19</sub> -C <sub>20</sub>	1.086	1.100	0.930	C <sub>21</sub> -C <sub>22</sub> -C <sub>23</sub>	121.31	121.19	120.20	C <sub>21</sub> -C <sub>22</sub> -C <sub>23</sub> -C <sub>24</sub>	0.000	0.0	0.5
C <sub>19</sub> -C <sub>21</sub>	1.465	1.461	1.455	C <sub>22</sub> -C <sub>23</sub> -C <sub>24</sub>	119.96	119.98	121.00	C <sub>22</sub> -C <sub>23</sub> -C <sub>24</sub> -C <sub>25</sub>	0.001	0.0	-0.6
C <sub>21</sub> -C <sub>22</sub>	1.407	1.406	1.394	C <sub>23</sub> -C <sub>24</sub> -C <sub>25</sub>	119.60	119.59	119.50	C <sub>23</sub> -C <sub>24</sub> -C <sub>25</sub> -C <sub>26</sub>	-0.001	0.0	0.8
C <sub>22</sub> -C <sub>23</sub>	1.387	1.387	1.373	C <sub>24</sub> -C <sub>25</sub> -C <sub>26</sub>	119.79	119.85	119.10	C <sub>24</sub> -C <sub>25</sub> -C <sub>26</sub> -C <sub>21</sub>	-0.001	0.0	-0.8
C <sub>23</sub> -C <sub>24</sub>	1.402	1.402	1.390	C <sub>25</sub> -C <sub>26</sub> -C <sub>21</sub>	121.33	121.16	121.90	C <sub>25</sub> -C <sub>26</sub> -C <sub>21</sub> -C <sub>22</sub>	0.002	0.0	0.7
C <sub>24</sub> -C <sub>25</sub>	1.403	1.403	1.381	C <sub>26</sub> -C <sub>21</sub> -C <sub>19</sub>	122.97	121.95	119.57	C <sub>26</sub> -C <sub>21</sub> -C <sub>22</sub> -C <sub>23</sub>	-0.002	0.0	-0.5
C <sub>25</sub> -C <sub>26</sub>	1.391	1.391	1.388	C <sub>21</sub> -C <sub>22</sub> -H <sub>29</sub>	119.27	119.50	119.9	C <sub>19</sub> -C <sub>21</sub> -C <sub>22</sub> -H <sub>29</sub>	-0.003	0.0	0.4
C <sub>26</sub> -C <sub>21</sub>	1.403	1.404	1.381	C <sub>24</sub> -C <sub>23</sub> -H <sub>30</sub>	118.60	121.42	119.4	C <sub>21</sub> -C <sub>22</sub> -C <sub>23</sub> -H <sub>30</sub>	180.00	180.0	-179.5
C <sub>22</sub> -H <sub>29</sub>	1.087	1.088	0.931	C <sub>25</sub> -C <sub>26</sub> -H <sub>27</sub>	119.98	120.14	119.0	C <sub>19</sub> -C <sub>21</sub> -C <sub>26</sub> -H <sub>27</sub>	0.003	0.0	-0.1
C <sub>23</sub> -H <sub>30</sub>	1.085	1.085	0.930	C <sub>24</sub> -C <sub>25</sub> -H <sub>28</sub>	120.85	120.90	120.4	C <sub>21</sub> -C <sub>26</sub> -C <sub>25</sub> -H <sub>28</sub>	-179.99	180.0	179.1

C <sub>25</sub> -H <sub>28</sub>	1.084	1.084	0.930	C <sub>24</sub> -O <sub>31</sub> -C <sub>32</sub>	118.37	118.37	117.8	C <sub>22</sub> -C <sub>23</sub> -C <sub>24</sub> -O <sub>31</sub>	-179.99	-180.0	179.9
C <sub>26</sub> -H <sub>27</sub>	1.085	1.085	0.930	O <sub>31</sub> -C <sub>32</sub> -H <sub>33</sub>	111.61	111.58	109.5	C <sub>23</sub> -C <sub>24</sub> -O <sub>31</sub> -C <sub>32</sub>	-179.99	-180.0	177.4
C <sub>24</sub> -O <sub>31</sub>	1.364	1.364	1.359	O <sub>31</sub> -C <sub>32</sub> -H <sub>34</sub>	105.89	105.86	109.4	C <sub>24</sub> -O <sub>31</sub> -C <sub>32</sub> -H <sub>33</sub>	61.12	61.20	63.3
O <sub>31</sub> -C <sub>32</sub>	1.418	1.419	1.427	O <sub>31</sub> -C <sub>32</sub> -H <sub>35</sub>	111.61	111.58	109.5	C <sub>24</sub> -O <sub>31</sub> -C <sub>32</sub> -H <sub>34</sub>	179.99	179.99	-176.8
C <sub>32</sub> -H <sub>33</sub>	1.098	1.097	0.960	N <sub>18</sub> -N <sub>16</sub> -H <sub>17</sub>	111.73	120.04	120.0	C <sub>24</sub> -O <sub>31</sub> -C <sub>32</sub> -H <sub>35</sub>	-61.21	-61.20	-56.7
C <sub>32</sub> -H <sub>34</sub>	1.091	1.091	0.960	N <sub>16</sub> -C <sub>14</sub> -O <sub>15</sub>	123.03	122.56	120.2	C <sub>19</sub> -N <sub>18</sub> -N <sub>16</sub> -H <sub>17</sub>	-179.99	0.0	-5.0
C <sub>32</sub> -H <sub>35</sub>	1.098	1.097	0.960	C <sub>1</sub> -C <sub>6</sub> -O <sub>7</sub>	119.30	119.44	120.1	C <sub>21</sub> -C <sub>19</sub> -N <sub>18</sub> -N <sub>16</sub>	-179.99	180.0	178.5
O <sub>7</sub> ...H <sub>17</sub>	1.902	1.923	1.94	N <sub>16</sub> -H <sub>17</sub> ...O <sub>7</sub>	135.22	132.80	134.0	N <sub>16</sub> -H <sub>17</sub> ...O <sub>7</sub> -H <sub>13</sub>	179.96	179.99	180.0

Table-3. Calculated vibrational wavenumbers, measured IR and Raman band positions (cm<sup>-1</sup>) and assignments for DMBBH

<i>Cis</i> $\nu_{\text{cal}}$	<i>Trans</i> $\nu_{\text{cal}}$	Relative intensity		Experimental			PED(%)
		IR	Raman	IR	Raman	Raman Solution	
3589	3587	8.99	0.42	3250 mbr	3270 vw	$\nu_{\text{O9H10}}(100)$ , $\nu_{\text{OH}}(\dots\text{O})$ , $\nu_{\text{NH}}(\dots\text{O})$ , $\nu_{\text{OH}}(\dots\text{N})$	
3582	3581	9.14	0.56	3200 mbr	3210 vw	$\nu_{\text{O7H13}}(100)$ , $\nu_{\text{OH}}(\dots\text{O})$ , $\nu_{\text{NH}}(\dots\text{O})$ , $\nu_{\text{OH}}(\dots\text{N})$	
3446	3352	10.9	1.99	3160 mbr		$\nu_{\text{NH}}(100)$ , $\nu_{\text{OH}}(\dots\text{O})$ , $\nu_{\text{NH}}(\dots\text{O})$ , $\nu_{\text{OH}}(\dots\text{N})$	
3091	3091	1.05	0.64			$2\nu_{\text{CH}}$ of Ph2(95)	
3082	3085	1.89	0.5			$2\nu_{\text{CH}}$ of Ph1(99)	
3078	3078	0.4	0.63	3074 wsh	3076 w	20a $\nu_{\text{CH}}$ of Ph2(100)	
3071	3072	1.2	0.8	3067 wsh	3065 wsh	7b $\nu_{\text{CH}}$ of Ph1(83)	
3067	3071	1.7	0.32		3048 vw	20b $\nu_{\text{CH}}$ of Ph1(94)	
3061	3036	2.56	0.34	3011 w	3012 vw	20b $\nu_{\text{CH}}$ of Ph1(91)	
3042	3016	5.26	1.07	2988 vw	2988 vw	$\nu_{\text{asy CH}_3}(100)$	
3015	3008	3.62	0.69			20b $\nu_{\text{CH}}$ of Ph2(99)	
3009	2949	7.02	0.36	2954 vw	2954 vw	$\nu_{\text{asy CH}_3}(100)$	

				2942 vw	2942 vw		VC19-H20
2946	2894	6.42	0.42				
			0.79	2912 vw	2912 vw		VC19-H20(94)
2890	2892	15.2		2902 vw	2902 vw		$v_{\text{sym}} \text{CH}_3(100)$
			5				
1666	1695	51.1		1631 s			$v_{\text{C=O}}(63), \delta_{\text{H17-N16-N18}}(13)$
			52.18				
1622	1624	0.8			-		$v_{\text{C18=N19}}(32), v_{\text{C-C}}(40)$
			14.08				
1613	1609	49		1605 vs	1609 vvs	1609 vvs	8b $v_{\text{C-C}} \text{Ph}_2(51)$
			100.0				
1598	1600	28.3			1588 msh		8a $v_{\text{C-C}} \text{Ph}_1(38), v_{\text{C18-N19}}(21)$
			1.11				
1585	1582	2.46		1576 vs	1574 vs	1574 vs	8a $v_{\text{C-C}} \text{Ph}_2(50)$
			13.59				
1565	1557	4.34		1556 vs	1558 vs	1559 vs	8b $v_{\text{C-C}} \text{Ph}_1(55) + \delta_{\text{CCH}} \text{Ph}_1(10)$
			17.98				
1532	1548	64		1536 wsh			$\delta_{\text{CNH}}(47), \delta_{\text{CCH}}(14)$
			8.27				
1509	1504	5.73		1514 vvs	1514 m	1515 m	19a $v_{\text{CC}} \text{Ph}_1(15) + \delta_{\text{CCH}} \text{Ph}_1(47)$
			2.06				
1503	1498	52.4					19b $v_{\text{CC}} \text{Ph}_2(11) + \delta_{\text{CCH}} \text{Ph}_2(33)$
			0.46				
1478	1473	13		1463 m	1463 wsh	1460 w	$\delta_{\text{HOC}}(60), \delta_{\text{CH}_3 \text{asy}}(22)$
			1.03				
1466	1460	0.93		1454 wsh	1453 w		$\delta_{\text{CH}_3 \text{sym}}(72), \delta_{\text{HOC}}(22)$
			0.43				
1446	1441	4.34		1436 vvw	1436 w		$\delta_{\text{CH}_3 \text{umbrella mode}}(82)$
			3.82				
1438	1433	7.27		1424 m	1424 m	1424 m	19a $v_{\text{CC}} \text{Ph}_2(41)$
			2.71				
1412	1410	1.27		1390 w	1384 w		19b $v_{\text{CC}} \text{Ph}_1(40), \delta_{\text{HCC}}(30)$

1359	1356	3.17	1.38	1366 w	1362 wbr		$\delta_{\text{H20 C19 N18}}(55)$
1345	1341	4.85	0.26	1359 wsh			$v_{\text{CO}}(36), v_{\text{CC Ph2}}(11), \delta_{\text{HCC}}(19)$
1313	1307	10.5	0.1	1335 vw			$14v_{\text{CC Ph2}}(57), \delta_{\text{HOC}}(26)$
1309	1305	13.8	10.03	1310 m	1312 m	1313 w	$v_{\text{CC Ph1}}(50)$
1294	1293	0.46	1.07	1279 vs	1278 m	1278 m	$14v_{\text{CC Ph1}}(56), \delta_{\text{CCH Ph1}}(28)$
1270	1267	5.25	0.38	1258 ssh	1259 m	1257 m	$3 \delta_{\text{CCH Ph2}}(31), v_{\text{CC Ph2}}(22), v_{\text{CO}}(11)$
1255	1253	49.6	2.96	1250 vvs			$v_{\text{C24-O31}}(42)$
1242	1223	100	10.08		1240 m	1241 m	$v_{\text{C=N}}(20), v_{\text{CC}}(16)$
1212	1212	31	58.28	1220 m			$3 \delta_{\text{CCH Ph1}}(32), \delta_{\text{HCN}}(11), \delta_{\text{HCC}}(11)$
1184	1180	7.95	0.57	1212 msh	1213 wsh	-	$15 \delta_{\text{HCC Ph2}}(40), v_{\text{CC Ph2}}(21)$
1176	1172	30.1	0.25	1193 m			$1 v_{\text{CC Ph2}}(56), \delta_{\text{HOC}}(10), \delta_{\text{HCC}}(10)$
1173	1169	2.52	0.53	1179 s	1179 m	1180 m	$\delta_{\text{CCH}}(20), \tau_{\text{OCH3}}(61)$
1156	1156	21.2	11.96	1172 m	1171 m	1173 m	$9a \delta_{\text{CCH Ph1}}(43), \delta_{\text{HOC}}(10)$
1153	1150	23.3	2.27	1152 m	1152 s	1152 m	$\delta_{\text{HOC}}(29), \delta_{\text{HCC}}(16)$
1142	1137	0.12	0.24				$\delta_{\text{HCH}}(22), \tau_{\text{CH3}}(77)$
1133	1130	26.3	26.41				$v_{\text{C-N}}(12), v_{\text{N-N}}(19), \delta_{\text{HCC}}(14)$
1099	1099	6.88	0.69	1104 s	1103 w	-	$18a \delta_{\text{HCC Ph1}}(57), v_{\text{CC Ph1}}(14)$

1081	1078	6.93	1.67	1074 m	1073 m	1072 w	18b $\delta_{\text{HCC}}$ Ph2 (24), $\delta_{\text{CCC}}$ Ph2(14)
1039	1057	5.92	2.95			-	$\nu_{\text{O31-C32}}$ (73)
1001	1034	12.4	0.56	1024 s			$\nu_{\text{N16-C14}}$ (27), $\nu_{\text{N16-N18}}$ (37)
991	988	0.02	0.17	984 w	984 w	984 vw	15 $\delta_{\text{CCH}}$ Ph1(61)
971	961	3.86	1.05	956 w			$\tau_{\text{HCNN}}$ (82)
965	958	0.17	0.07	950 vw	950 vvw	948 vw	10a $\delta_{\text{CCC}}$ Ph2 (32), $\nu_{\text{CO}}$ (21), $\delta_{\text{CCC}}$ (22)
958	942	1.2	0.86				$\tau_{\text{HCCC}}$ (77)
929	929	0.38	0.24	930 vw			17a $\delta_{\text{CCH}}$ Ph1(70), $\tau_{\text{CCCH}}$ Ph1(17)
920	908	0.58	0.01	918 vw	918 w	924 vw	10a $\delta_{\text{CCH}}$ Ph1 (79)
915	894	3.8	0.83				$\delta_{\text{OCN}}$ (20), $\delta_{\text{CNN}}$ (31)
836	829	3.71	0.45	853 m	855 vw	854 w	$\nu_{\text{CC}}$ Ph1(42)
815	812	6.46	0.13	826 m	825 vw		$\tau_{\text{CCCC}}$ Ph1 (71)
812	811	5.29	0.13	807 vw	808 vw		10b $\delta_{\text{HCC}}$ Ph2(78)
798	797	0.01	0.4	790 w			$\delta_{\text{HCC}}$ Ph1(35), $\delta_{\text{OPCOH}}$ (35)
762	759	0.47	2.93	774 vw	775 w	774 vw	$\delta_{\text{CC}}$ Ph1(15), $\delta_{\text{CO}}$ (19)
747	746	6.44	0.53	756 m	750 w	750 vw	$\tau_{\text{HCCC}}$ Ph2(44), $\tau_{\text{CCCC}}$ (13), $\tau_{\text{OCCC}}$ (22)
731	728	0.88	2.01	736 w	738 w		4 $\nu_{\text{CC}}$ Ph2 (19), $\nu_{\text{CO}}$ (16), $\delta_{\text{CCC}}$ Ph2 (53)

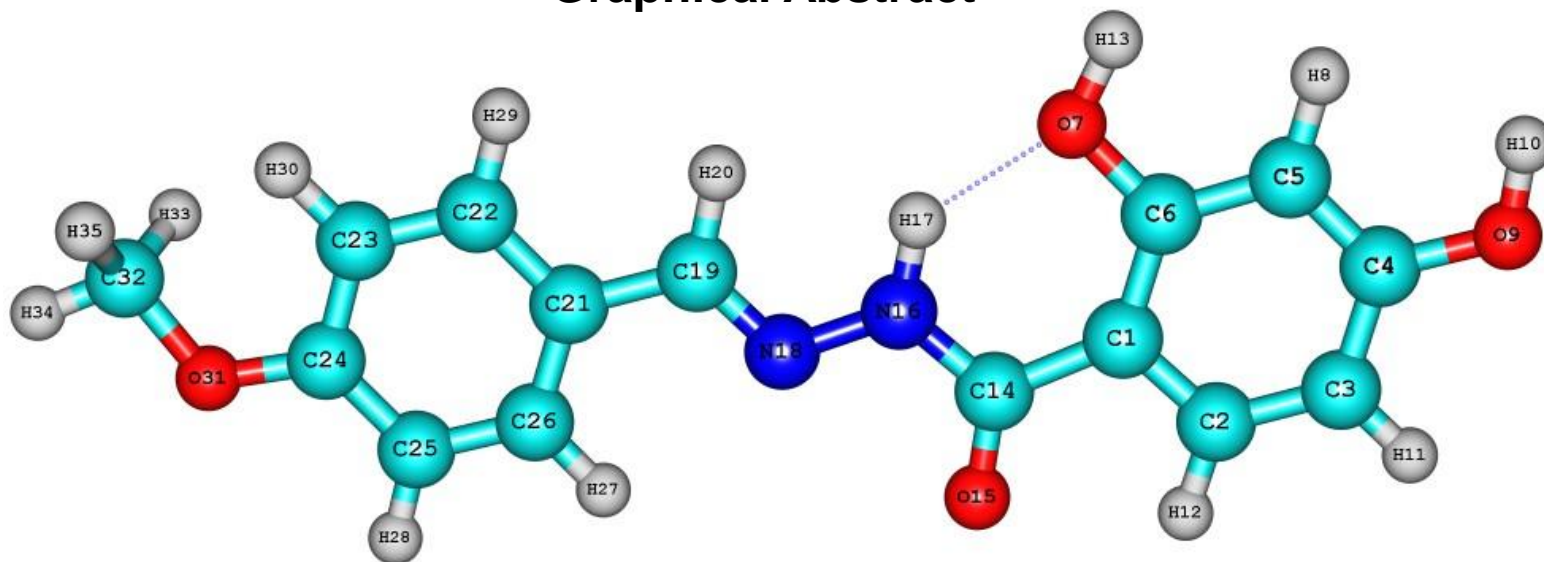
721	720	0.07	0.18				$\tau_{\text{HNCC}}(13), \tau_{\text{HCCC Ph2}}(14) \delta_{\text{op ONCC}}(58)$
705	702	0.14	0.21	690 vw	692 vw		$4\tau_{\text{HCCPh1}}(59), \delta_{\text{op CCC}}(13)$
663	653	0.22	0.03	647 s	646 w		$6a \tau_{\text{CCCC Ph2}}(17), \tau_{\text{HNCC}}(26), \tau_{\text{HCCC Ph2}}(12),$ $\delta_{\text{op CCC}}(14)$
629	626	0.08	0.88	634 vw	632 w		$v_{\text{NN}}(10), \delta_{\text{CCC Ph1, Ph2}}(29)$
623	611	0.88	0.02	619 m	620 w	619 vw	$v_{\text{CCPh1, Ph2}}(11), \delta_{\text{CCC Ph1 Ph2}}(43)$
623	606	3.18	0.18	605 m			$\tau_{\text{HNCC}}(25), 6b \delta_{\text{CCCC Ph2}}(15), \delta_{\text{op CCC Ph2}}(40)$
597	596	5.18	0.21	572 w	571 w		$\delta_{\text{CNH}}(32), \delta_{\text{op NCC}}(13) \delta_{\text{op CCC}}(34)$
582	549	13.8	0.33				$\delta_{\text{OCC}}(24)$
545	545	0.51	0.73	539 wsh	536 w		$\delta_{\text{CCC Ph1, ph2}}(34)$
526	524	1.1	0.07	528 mbr	530 wsh		$\tau_{\text{CCCC Ph1}}(10), \tau_{\text{NNCC}}(32), \delta_{\text{op CCCC Ph1}}(15)$
521	517	0	0.99	492 w	489 w	491 vw	$v_{\text{C-O}}(11), 16a \delta_{\text{CCC Ph2}}(19) \delta_{\text{op OCC Ph2}}(21)$
491	499	3.35	1.11	475 vw	478 vw		$\delta_{\text{OCC}}(17), \delta_{\text{COC}}(22)$
447	447	0.55	0.02	463 vw	464 vw		$\tau_{\text{OHCCC}}(14), 16b \tau_{\text{OCCCC Ph2}}(45), \delta_{\text{op OCC Ph2}}(24)$
424	419	0.38	0.26	456 vw	457 vw		$\delta_{\text{OCN}}(23), \delta_{\text{CCN}}(16) \delta_{\text{CCC Ph1}}(13)$
413	410	0.1	0.22	422 vw	425 w	424 vw	$16b \tau_{\text{CCCC Ph1}}(62)$
399	400	7.41	0.83		395 w		$16a \tau_{\text{CCCC Ph1}}(41), \tau_{\text{CNCC}}(16), \delta_{\text{op OCC}}(14)$
398	393	0.16	0.71				$\delta_{\text{OCC}}(14), \delta_{\text{CCC Ph1, Ph2}}(11), \delta_{\text{NCC}}(17),$ $\delta_{\text{CCN}}(12)$

360	354	0.84	0.1			$v_{CC}(15), \delta_{CCC} \text{ Ph1, Ph2 (34)}$
			0.77			
358	351	19				$\tau_{OHCC}(94)$
			0.19			
343	338	1.88		329 w	332 vw	$\delta_{CCC} \text{ Ph2(15), } \delta_{OCC}(76)$
			0.13			
315	318	5.86				$\tau_{OHCC}(18), \tau_{CCC} \text{ Ph2(39)}$
			1.19			
290	275	0.83		274 w		$\delta_{OCN}(13), \delta_{CCC} \text{ Ph1, ph2(31) } \delta_{CNN}(14)$
			0.94			
277	274	16.7				$\tau_{OHCC} (55), \tau_{NNCC}(10)$
			0.18			
258	256	0.27		238 w		$\tau_{OHCC}(14) \tau_{HCOC} (30), \tau_{NNCC}(12)$
			0.32			
246	228	0.64				$\delta_{ECC}(11), \delta_{OCC}(33), \delta_{COC}(29)$
			0.99			
228	228	0.78				$\tau_{HCOC}(32), \tau_{NNCC}(16), \tau_{op} \text{ cccc}(16)$
			0.75			
216	216	0.14		205 w		$\tau_{CCCC}(66), \delta_{op} \text{ occc}(26)$
			0.21			
190	198	0.34				$\tau_{NNCC}(26), \tau_{CCCC}(20)$
			0.4			
153	193	0.04		165 vw		$\tau_{CCCC} (16), \tau_{CNNC} (17), \tau_{CCCN}(21)$
			0.23			
131	122	0.42				$\tau_{CCCC}(45)$
			0.88			
120	106	0.34				$\tau_{CCCN}(52)$
			2.45			
97	100	0.03				$\tau_{CCCC}(40)$
			0.58			
69	78	0.82				$\tau_{NNCC}(38)$
			4			
45	47	0.37				$\tau_{CNNC}(62)$

41	35	0.48	1.26	$\tau_{CCCC}(52)$
27	22	0.03	2.23	$\tau_{CCCC}(35)$
17	20	0.39	0.07	$\tau_{CCCN}(45)$

---

## Graphical Abstract



The experimental and theoretical vibrational analysis of 2,4-dihydroxy-*N'*-(4-methoxybenzylidene)benzohydrazide has been performed. The molecular geometry, vibrational wavenumber, infrared and Raman intensities of the molecule in the ground state have been calculated by using DFT method. The NBO analysis explained the intramolecular hydrogen bonding and the hyperconjugative interaction. Information about the size, shape, charge density distribution and site of chemical reactivity of the molecules has been obtained by mapping electron density isosurface with electrostatic potential surfaces (ESP). A complete vibrational analysis has been attempted on the basis of experimental infrared and Raman spectra and calculated vibrational modes and potential energy distribution over the internal coordinates.

### Highlights

- Vibrational spectra of the 2,4-dihydroxy-N'-(4-methoxybenzylidene)benzohydrazide have been analysed.
- The computed vibrational wavenumbers were seen to be in good agreement with the experimental data.
- Conformation analysis
- The natural bond orbital (NBO) analysis has been carried out.

ACCEPTED MANUSCRIPT